RECEIVED
LAWRENCE
RADIATION LABORATORY

MAR 5 1969

LIBRARY AND
DOCUMENTS SECTION

UCRL-18673

cy. 2

DIRECT OBSERVATION OF MOTION OF DISLOCATIONS IN DEFORMED SILICON BY X-RAY TOPOGRAPHY

Vugranam Chakravarthy Kannan
(Ph. D. Thesis)

January 1969

TWO-WEEK LOAN COPY

This is a Library Circulating Copy which may be borrowed for two weeks. For a personal retention copy, call Tech. Info. Division, Ext. 5545

LAWRENCE RADIATION LABORATORY
UNIVERSITY of CALIFORNIA BERKELEY

UCRL-18673 cy. 2

DISCLAIMER

This document was prepared as an account of work sponsored by the United States Government. While this document is believed to contain correct information, neither the United States Government nor any agency thereof, nor the Regents of the University of California, nor any of their employees, makes any warranty, express or implied, or assumes any legal responsibility for the accuracy, completeness, or usefulness of any information, apparatus, product, or process disclosed, or represents that its use would not infringe privately owned rights. Reference herein to any specific commercial product, process, or service by its trade name, trademark, manufacturer, or otherwise, does not necessarily constitute or imply its endorsement, recommendation, or favoring by the United States Government or any agency thereof, or the Regents of the University of California. The views and opinions of authors expressed herein do not necessarily state or reflect those of the United States Government or any agency thereof or the Regents of the University of California.

UCRL-18673

UNIVERSITY OF CALIFORNIA

Lawrence Radiation Laboratory
Berkeley, California

AEC Contract No. W-7405-eng-48

DIRECT OBSERVATION OF MOTION OF DISLOCATIONS IN DEFORMED SILICON BY X-RAY TOPOGRAPHY

Vugranam Chakravarthy Kannan

(Ph.D. Thesis)

January, 1969

TABLE OF CONTENTS

ABSTRACT

I. INTRODUCTION 1

II. EXPERIMENTAL PROCEDURE 5

A. Specimen Preparation 5

B. Mode of Deformation and Loading System 5

C. Observation of Dislocations by X-ray Topography 7

D. Measurement of Dislocation Velocities 10

E. Transmission Electron Microscopy 11

III. EXPERIMENTAL RESULTS 13

A. Characteristics of Dislocation Motion 13

B. Propagation of Dislocations at High Temperature 13

C. Annealing of Dislocations at High Temperature 14

D. Deformation Under Tension 15

E. Electron Microscopic Investigation 17

F. Motion of Individual Dislocations and Measurements of Dislocation Velocities 18

IV. DISCUSSION 25

A. Nucleation and Generation of Dislocations 25

B. Propagation of Dislocations at High Temperatures 26

C. Effect of Aging on Dislocation Mobilities 29

D. Electron Microscopic Investigation 30

E. Mobilities of Individual Dislocations 32

1. Pinning of Moving Dislocations 32

2. Thermally Activated Process 35

3. Activation Energy for Glide Motion 37

V. CONCLUSIONS 42

APPENDIX 43

ACKNOWLEDGEMENT 45

REFERENCES 46

FIGURE CAPTIONS 48

FIGURES 54

DIRECT OBSERVATION OF MOTION OF DISLOCATIONS IN DEFORMED SILICON BY X-RAY TOPOGRAPHY

Vugranam Chakravarthy Kannan

Inorganic Materials Research Division, Lawrence Radiation Laboratory
Department of Material Science and Engineering, College of Engineering
University of California, Berkeley, California

ABSTRACT

Measurements of glide velocities of isolated individual dislocations as a function of temperature in the range 775°-920°C were made in silicon single crystals by x-ray Lang topography and the data was correlated with the appearance of the dislocation lines. Qualitative information was also obtained on the mobilities of dislocations at temperatures around ~1000°C as well as on the generation and multiplication of dislocations during the initial stages of plastic deformation in highly perfect crystals.

Under stresses far below the macroscopic yield point, dislocation generation invariably took place at or near the surfaces. Vacancy clusters or loops in a few quenched and aged specimens did not act as sources but rather were obstacles to the passage of dislocations. Although the average direction of all dislocations was along ⟨110⟩ none of the lines were perfectly straight suggesting that the Peierl's stress is not high enough to align the dislocations along the close-packed directions.

The mobilities of dislocations generated at high temperatures (~1000°C) were greatly diminished at lower temperatures (~825°C). Further motion of such high-temperature dislocations always resulted in avalanche-like multiplication giving rise to bands of dislocations. The individual dislocations in these bands were not resolved in the x-ray topographs. Electron microscopic investigation of the detailed configuration of dislocations in

these bands indicates that the damage left behind by the moving dislocations was exclusively in the form of opposite dislocation pairs or dipoles of various sizes distributed narrowly on the main slip plane.

The immobilization of dislocations exposed to high temperatures was attributed to the developments of jogs on the dislocation lines during their motion. A possible mechanism for jog formation due to the climb of a short segment of a nearly straight screw dislocation is proposed.

The apparent activation energy for the dislocation motion was found to be 1.8 ± 0.3 e.v. for screw and 60°- dislocations at a constant stress of 36 gm/mm^2: Careful observation of the appearance of dislocation lines showed that they are not straight but are pinned uniformly along their lengths and the pinning distances varied inversely with temperature. These pinning points were tentatively attributed to the presence of thermal jogs on the dislocation line. A plot of logarithm of pinning distances against the reciprocal of temperature yielded an activation energy of ~1.2 e.v., which is identified with the jog-formation energy in silicon.

Detailed analysis of the velocity data lead to the conclusion that the forward motion of jogs is not the rate controlling process for dislocation glide in the present case; rather the presence of jogs very well account for the observed shapes of the dislocation lines. Accordingly, the activation energy for dislocation motion was identified with the energy required for kink-pair nucleation and migration. Formulation of forward velocity of a straight dislocation in terms of kink nucleation and migration is presented in the Appendix. The resulting velocity equation shows that the measured activation energy of ~1.8 ± 0.3 e.v. for dislocation motion should equal the arithmatic mean of the energies required for kink-pair nucleation and migration.

Assuming a "quasi-parabolic" form of potential, the Peierl's stress τ_p was computed from the pre-exponential term to be 1.76×10^{10} dynes/cm^2. Under small applied stresses, this leads to the velocity-stress dependence as $v \sim \tau^2$, which is identical to the observed relationship in silicon by previous workers.

I. INTRODUCTION

Measurements of velocities of individual dislocations are of particular interest in the study of the dislocation theory of the flow stress, solution hardening, creep and other plastic properties of pure and slightly impure single crystals. Gilman and Johnston[1] were the first to develop an etch-pitting technique for the measurement of dislocation velocities in LiF. They measured the speeds of individual edge and screw dislocations as a function of the applied stress. Shortly thereafter, by employing this technique with slight modifications, speeds of individual dislocations were measured in a number of cyrstals. Stein and Low[2] conducted experiments in silicon-iron, Chaudhuri[3] et al. in several semi-conducting materials, Kabler[4] and Haasen[5] in germanium, Marukawa[6] in copper and in several other materials by various investigators.[7-10] A striking observation made by all these investigators was that dislocations seldom moved uniformly in the crystal. Even in the same area under observation, dislocations having the same burger's vectors moved with different speeds, from very slow to fairly fast. As a result, every recorded value of dislocation velocity by these authors is an average of 40 to 100 dislocations that moved to various extents under the same applied stress pulse. The main difficulty with such an approach is that the true meaning of the seemingly fundamental relationship between stress and dislocation velocity becomes unclear and vague if the characteristics of the moving dislocations are not well known. For example, jogs on a moving screw dislocation must be dragged non-conservatively and even on edge dislocations jogs greatly reduce mobility. This dragging force on the moving dislocation

is dependent on the jog density and the heights of the jogs but very little quantitative infromation on this is available. Qualitative observations by Young and Sherril[11] and by Petrof and Washburn[12] in copper have shown that heavily jogged dislocations do require higher stresses for motion than do relatively jog-free dislocations. Also, in real crystals dislocations are rarely straight. The etch-pit technique cannot give information regarding the radius of curvature of the moving dislocation; another difficulty is that etch-pit displacements are equal to the distance moved by the dislocation perpendicular to itself only when the dislocation intersects the trace of the glide plane on the surface of observation at right angles. The etch-pit technique does not give information regarding this angle.

X-ray topography is a powerful technique for the direct observation of dislocations in nearly perfect crystals. It can only be used with undeformed or lightly deformed good quality crystals with dislocation densities less than 10^4 dislocations/cm^2. This is due to the poor resolution of the technique which is of the order of $4\ \mu$. Measurements of positions of individual dislocations made repeatedly after motion at different temperatures and applied stresses can give unambiguous information on glide velocity. Since it is possible to observe the whole dislocation, the characteristics of the dislocation i.e. edge, screw, straight or curved etc. can be correlated with the velocity data.

Although the above considerations apply to all crystalline materials, the present investigation was undertaken to study the motion of isolated individual dislocations in highly perfect silicon single crystals. Silicon was chosen as the test material for various reasons. It is available as a semi-conductor material of high chemical purity and crystal

perfection (of nearly zero dislocation density). In crystals with the diamond cubic structures such as silicon, dislocations are immobile at room temperature. They become mobile gradually above about 0.5 Tm where Tm is the temperature of melting. This is an important experimental advantage because by simple rapid cooling, any dislocation configuration can be frozen in place for observation at room temperature. The speeds of dislocations in these materials vary slowly with applied stress,[13] for example, roughly as σ^{2} to $\sigma^{1.5}$ at higher stress levels and $\sigma^{3.5}$ at lower stress levels. This dependence can be contrasted with an estimated σ^{200} in case of copper[14] and σ^{25} and σ^{44} measured directly in Lif[1] and silicon-iron[2] respectively. Thus, experimentally, it is relatively easier to control the velocity of dislocations in silicon as compared to metals.

Mobility of dislocations in silicon and germanium, both as a function of applied stress and temperature, has been studied by the etch-pit technique by Kabler[4], Haasen[5] and Chaudhuri[3] et al. and by x-ray topography by Suzuki and Kojima[15]. These results on dislocation motion and internal friction data in semi-conductors have been explained in terms of the Peierls' mechanism of dislocation glide i.e. formation and propagation of double-kinks along the dislocation lines. In order to explain Kabler's data on dislocation velocities in germanium, Celli et al.[1] recently modified the simple Peierl's model by assuming that discrete dragging points along the dislocation line could affect kink-nucleation; they did not elaborate on the nature of these dragging points nor on the mechanism of their formation. Suzuki and Kojima[15] who studied dislocation motion in silicon by x-ray topography, however, did not find any evidence concerning the barriers against kink nucleation and propagation. Different

amounts and species of impurities did not affect their velocity data in the temperature range they investigated i.e. 600°-800°C.

The main purpose of the present investigation was to observe the motion of individual isolated dislocations to obtain more reliable data on temperature dependence of the velocities, which would be correlated with the appearance of the dislocation lines i.e. straight, wavy or curved, edge or screw. In the course of the experiment it was hoped that information would also be obtained on the nature of dislocation sources and on the multiplication and the distribution of dislocations during the early stages of plastic deformation of highly perfect silicon single crystals.

II. EXPERIMENTAL PROCEDURE

A. Specimen Preparation

High purity silicon single crystals were obtained from the Texas Instruments Co. in the form of cylindrical rods of 1 in. dia. × 6in. long. The Table I gives the specifications of the crystals such as mode of crystal preparation, specific electrical resistivities, initial dislocation densities etc. Wafers of 45 mil thick were cut from the original stock with [111] [110] or [112] orientations by a wire-saw using 800 mesh silicon carbide as abrasive or with a diamond wheel. In order to remove the surface damage introduced while cutting, the wafers were chemically polished to a depth of ten microns. The polishing solution used was of the following composition[17]:

A freshly prepared mixture of 65% A and 35% B where

(A) is 3:1 mixture of concentrated HNO_3 and 48% HF and

(B) is 2.5 gm of iodine in 1100 ml of glacial acetic acid.

After polishing, the wafers were washed in copious amounts of water containing sodium bi-carbonate, then in alcohol and dried. The final thickness of the wafers varied from 40 to 43 mil. X-ray topographs of a few untreated wafers showed that these crystals were free of dislocations within the limits of experimental observation.

Tensile specimens of desired orientations were cut from the wafers in an ultrasonic cutting machine. The specimen geometry is depicted in Fig. 1. The specimens were once again chemically polished to round-off the sharp corners and also to remove any damage introduced during ultrasonic cutting.

B. Mode of Deformation and Loading System

Fresh dislocations were introduced into the crystals by pressing a

TABLE I.

Method of Preparation	Growth axis	Resistivity Ω - cm	Type of conductivity	Initial Disc. Density cm^2
Czechrolski	[111]	50	N	nearly zero

molybdenum pointer on the surface of the specimen at 1000° - 1050°C for 15-30 minutes. This was carried out either in vacuum of 10^{-6} mm of Hg at the operating temperature or in an atmosphere of high purity helium. Long dislocations were generated from the point of contact and moved into the specimens. The number of dislocations generated and the distance to which they moved depended on temperature, load and loading time. An example is shown in Fig. 2.

The tensile deformation was also carried out either in vacuum or in helium atmosphere. Since silicon is extremely brittle at room temperature, a special jig made of molybdenum was employed to grip the specimens. Dead loading was employed for times ranging from ten minutes to one hour. A maximum of 2.5 K gm was possible to apply by this method. Provisions were available to load or unload at high temperatures. The resolved shear stress was calculated from the knowledge of the total load applied and the geometry of the specimen. The temperature of the specimen was read by a chromel-alumel thermocouple placed at a distance of 5 mm. The recorded temperature was within ± 1°C of the appropriate test temperature and the specimen temperature was regulated within ± 5°C. After the test, the specimens were cooled rapidly to room temperature in vacuum under the load.

C. Observation of Dislocations by X-ray Topography

In principle, there are two different ways by which x-ray topography in transmission can be employed. One technique is to make use of the phenomenon of primary extinction (developed by Lang)[18], while the other takes advantage of anomalous transmission of x-rays (Bormann technique)[19]. In the present studies, we have employed the former technique. Anomalous transmission is useful for the study of imperfections in nearly perfect metallic crystals because the mass absorption coefficients (μ) for commonly

employed x-ray wavelengths are high. For example, to study imperfections in a copper crystal in transmission by the extinction technique, (the Lang method) the limiting thickness of the sample would be only about 50 microns, but anomalous transmission makes it possible to use even 1 mm thick specimens. However, the crystals must be more perfect for anomalous transmission. Silicon samples of 1 mm thickness can be studied by the extinction technique because μ is very small ($\mu t = 1$ for thickness ~ 1 mm and for Mo K_{α_1} - radiation). The main drawbacks of the x-ray techniques are their poor resolution. In order to obtain intense and well localized images of dislocations by primary extinction, μt should not much exceed unity. An extensive review article on x-ray transmission topography and the advantages of the technique has recently been published by Webb[20].

The visibility of dislocations depends upon many factors. Pure screw dislocations are invisible when $g.b=0$ where g is the reciprocal lattice vector for the operating reflection and b the burgers vector of the defect. Pure edge dislocations vanish completely only when two conditions are satisfied i.e. $g \cdot b=0$ and $g \times n = 0$, where n is the unit vector tangential to the dislocation line.

The geometry of the experimental set-up is shown schematically in Fig. 3. S is a line source of x-radiation, of 1×1.4 mm dia. seen end-on, about 50 cm away from the sample to limit the horizontal divergence of the x-ray beam. V_2 is a stationary slit to stop the transmitted beam from striking the photographic plate P, which is placed at right angles to the diffracted beam as close to the sample as possible. The photographic plate will record only the area exposed by the slit V_1. In order to obtain the entire topograph of the wafer, the photographic

plate and the crystal have to be translated synchronously in the direction indicated by the arrow.

Figure 4 is a photograph of the Lang camera aligned with the x-ray tube on the Hilger Microfocus x-ray table. The specimen was mounted on the three-stage goniometer in Laue-geometry and rotated so as to obtain the desired $\vec{g}$-vector (operating reflection). A translation speed of 0.6 mm/min. was employed to obtain the topograph of the entire area of the specimen. The x-ray images were photographed using the Mo K_{α_1} - radiation. The tube was operated at 40 k.V., 3.0 m A. A 2.5 × 3.5 cm Ilford G-plate with 50μ emulsion thickness was used. Each plate needed an exposure time of roughly 20 minutes/mm of translation to give the best contrast.

The photographic plates were processed by a special developing procedure to obtain the best contrast conditions as follows[17]: The plates were first soaked in distilled water at 10°C for 10 minutes and then developed in D-19 at 10°C for 30 minutes, stirring the solution at least once for every five minutes. After rinsing in a stop-both (1% acetic acid solution) for ten minutes, the plates were fixed for 3 hours in a hardening fixer. They were then washed in running water for 3 hours, again rinsed in photo-flo and dried at room temperature for 5-6 hours.

Final prints were obtained from the nuclear plates by a two stage process. Positives were first taken onto the contrast process-ortho film and then the final enlargements were made from the film. Thus, all the topographs in this thesis are negatives i.e. dark regions on the print correspond to higher x-ray intensities on the plates. Topographs have been enlarged 10 to 20 times, although the resulting grain size allowed much higher magnifications.

D. Measurement of Dislocation Velocities

Topographs were taken before and after loading the specimen at a particular temperature for a specified length of time. The distance travelled by the dislocations was accurately measured as follows. The areas in the vicinity of the dislocation in question were carefully scrutinized to locate some reference points on the two topographs. Small black-dots due to surface imperfections or markings could serve best for this purpose. It was first assured that these dots themselves did not move during the test. This was done by checking the positions of the dots in the initial and final topographs with reference to the edges of the specimen. The distance moved by the dislocation perpendicular to itself was computed by measuring its distance from the reference dots before and after testing. Knowing the duration of load-application, the average velocity of the dislocation was calculated. A few examples will be cited for illustration.

The dislocation numbered 1 in Fig. 18(a) can be identified in Fig. 18 (b) after stressing. The dots marked (A) and (B) in these topographs are taken as the reference points. While the dislocation line was above A and B in Fig. 18(a), it moved right onto these dots in Fig. 18(b). On further continuation of the test, the line moved past the dots A and B as shown in Fig. 18(c). As another example, two dislocations numbered 4 and 5 in the Fig. 17(a) can be identified after their motion during the test in Fig. 17(b). Two black-dots marked A and B in Figs. 17(a) and (b) are taken as reference points. Observe that the dislocations 4 and 5 which are away from A and B in Fig. 17(a) moved right onto the dots in Fig. 17(b). Likewise, the motion of 60°- segments of these two dislocations can be compared with the dot marked C in Figs. 17(a) and (b).

All measurements were made on the final prints taking particular care to correct for any small differences in magnification of the various topographs. Only nominal magnifications are quoted in the figures captions. The exact magnification for each print is calculated by measuring the length of a long and well-defined dislocation line on the original nuclear plate with the help of a Bauch and Lomb Measuring Magnifier (accurate to 0.05 mm) and comparing this to the measured length of the same dislocation line in the print by Starrett Steel Rule with 0.5 mm graduation marks. Since the (111) - planes on which the dislocations moved were inclined to the surface of the specimen, the distances measured on the topographs were projected distances. The true distance travelled by the dislocations was calculated by knowing the angle subtended by the glide plane at the specimen surface. Since the image widths of dislocation lines were of the order of 25μ the error introduced into the measured total distance travelled by a dislocation line was minimized by comparing the topographs before and after the test several times for positions of equal contrast prior to making measurements.

E. Transmission Electron Microscopy

This technique was used to investigate the details of the damage left behind by moving screw dislocations because the resolution of the x-ray technique is inadequate. The experimental procedure for obtaining electron microscope foils was as follows[21]: square sections of 6 × 6 mm were cut from the 1 mm thick specimen by a hardened carbide scriber. The specimen was then polished for one hour at room temperature. The polishing solution was kept agitated during polishing to obtain a uniform final thickness. This procedure reduced the thickness from 40 mil to about 5 mil. Then the sample was thoroughly cleaned with water and degreased in boiling trichlo-

roethylene and then mounted on a teflon sheet with apiezon cement so that only one face was exposed. The second surface that was towards the teflon could not be attacked during subsequent polishing. The sheet was then immersed in the polishing solution again and chemical thinning was continued. The square sample not only was thinned in this process but its area also diminished considerably. When it reached the size of about 2 mm in diameter, it was thin enough to transmit visible light. The polishing was stopped at this stage, the sample was rinsed with water thorougly and placed in a bath of trichloroethylene to dissolve the apiezon. The foils were then washed in acetone and dried for observation in the electron microscope. The specimens were examined in a Siemens Elmiskop I equipped with a double tilt goniometric specimen holder.

III. EXPERIMENTAL RESULTS

A. Characterisitcs of Dislocation Motion

The initial dislocation density of all the specimens studied in the present investigation was zero within the limits of experimental observation. Hence, as a first step fresh dislocations were generated and then their propagation was studied under various conditions. Essentially, two types of studies were made. Firstly, dislocations were introduced by pressing a molybdenum pointer at about 1000° - 1050°C. Dislocations were generated at the point of compression and travelled a long distance into the specimen. In the second set of experiments, controlled motion of individual dislocations under extremely small applied tensile stress was observed. Velocities of isolated dislocations were measured at various temperatures. These will be described in the following paragraphs in detail.

B. Propagation of Dislocations at High Temperatures

Figures 5 to 8 are topographs of specimens in which dislocations were generated by pressing a molybdenum pointer at about 1000°C. The exact load applied and the temperature of deformation for each are given in the figure captions. It can be seen from these pictures that dislocations were generated in groups from the point of compression. Figures 5(a) and (b) are $\bar{1}\bar{1}1$ and $\bar{1}10$ topographs respectively. The dislocation lines at A are seen in both the topographs while those at B and C are seen in $\bar{1}\bar{1}1$ topograph but not in $\bar{1}10$ topograph. Thus, the burgers vector of the dislocation lines at B and C can be unambiguously assigned as $\frac{a}{2}[\bar{1}01]$. Observe that these screw dislocations exhibit extensive cross-slip as they moved towards the upper left-hand corner from the centre of the specimen (see Fig. 5(a)). Similarly, the dislocations at A in Fig. 6(a) and (b) are screws with

$b = \frac{a}{2}[0\bar{1}1]$. Note the elongation of the lines in the direction of the burger's vector. These dislocations also developed pinning points as they travelled from the centre towards the right-hand side as can be seen in Fig. 6(a). (One such pinning point on the dislocation line is shown at P.) Although it is difficult to see dislocations individually in the band A (Fig. 6(a)), closer observation reveals that the leading dislocation in the band developed a greater number of pinning points than the inner ones. Figure 7 is an example showing groups of long screw dislocations ($b = \frac{a}{2}[1\bar{1}0]$) which developed pinning points, cusps and even cross-over loops as they travelled in the crystal (see figure caption). These pinning points developed to various sizes and configurations as can be seen in Fig. 8. The dislocation lines at A ($b = \frac{a}{2}[\bar{1}01]$) are of particular interest in this topograph. Small pinning points, cusps, long cusps and well developed cross-over loops can be seen on the dislocations at A. These dislocation lines can be considered as long helices with the axis of the helix running parallel to the dislocation line.

C. Annealing of Dislocations at High Temperatures

Some specimens, after dislocations had been introduced by the above technique, were annealed at about 1000°C or above. Topographs (a), (b) and (c) of Fig. 9 show the dislocations generated by a molybdenum pointer which was pressed on a (112) surface at 1000°C while (d) (e) and (f) show the same area after annealing at 1050°C for 30 minutes. The internal stress was the driving force for dislocation motion during annealing. Nearly straight dislocations in (a) became curved and wavy (d), even though they did not move appreciable distances (b) and (e) are examples showing that long dislocations of nearly screw orientation ($b = \frac{a}{2}[110]$) became curved and bowed

out possibly on cross-slip planes exhibiting the characteristics of a dislocation tangle. In (c) some dislocations were generated, where some kind of hard particle pressed against the specimen inadvertently. Such dislocations are seen to have collapsed into the source, probably by glide, on heating to high temperature (see f).

D. Deformation Under Tension

Tensile specimens were cut from wafers in which dislocations had been introduced by a molybdenum pointer at 1000°C. Figure 10 shows a series of topographs of a specimen (surface orientation (112)) deformed in tension along $[\bar{1}10]$. Figure 10(a) is the topograph of the specimen showing dislocations introduced at high temperatures. Long dislocations running across the topograph at A have $b = \frac{a}{2}[0\bar{1}1]$. Figure 10(b) was taken after loading the specimen along $[\bar{1}10]$ at 850°C for 15 minutes. Observe that the old dislocations did not move while new dislocations were generated near the surface at many places. A similar experiment was conducted in another specimen of (110)-orientation. The topographs before and after deformation are shown in Fig. 11 (a) and (b) respectively. The applied tensile stress was 380 gm/mm^2. While the dislocations at A moved across the width of the specimen, curved ones at B did not move. Figure 12 is the topograph of the specimen cut from the crystal shown in Fig. 8. The specimen was pulled along $[\bar{1}10]$ at 850°C for 30 minutes under a tensile stress of ~200 gm/mm^2. Figure 12(a) shows the dislocation substructure of the specimen after the test. Note that no dislocations moved nor were any generated. (Compare Fig. 8 with Fig. 12(a)). The specimen was pulled again along $[\bar{1}10]$ at 950°C under a small tensile stress (20 gm/mm^2) and the topograph (Fig. 12(b)). Some dislocations climbed towards the specimen surface and even intersected

at the area B in Fig 12(b). When the specimen was once again loaded in tension under a stress of 380 gm/mm^2 at 900°C (see Fig. 12(c)), profuse generation of dislocations occurred from the edges of the specimen, but the high temperature dislocations still did not move.

A specimen with zero initial dislocation density was loaded to a tensile stress of 380 gm/mm^2 along [1$\bar{1}$0] at 850°C. A series of topographs were taken after various times. Figure 13 shows the enlarged topographs. It is evident that dislocations were mainly generated from the side surfaces or edges and travelled a long distance into the specimen with the screw segments lying roughly parallel to the surface. Dislocations were generated in groups and many of them are not straight. With progressive deformation, dislocation densities increased in the pile-ups eventually spreading thoughout the specimen. The individual dislocations are not well resolved especially in the final topograph of the series. If it is assumed that the resolving power of the technique is 4μ, the dislocation densities in these pile-ups correspond to at least 6×10^6 dislocations/cm^2. Another sample with zero initial dislocation density was deformed under a stress of 380 gm/mm^2 at slightly higher temperature of 920°C. Many dislocations were generated in groups through out the sample (Fig. 14). Again note that the side surfaces in edges of the sample were the nucleating centres. In a third sample, the deformation conditions were reversed, namely, stress of 30 gm/mm at 950°C. The dislocations generated under these conditions are shown in Fig. 15(a). The orientation of the specimen is shown in the figure itself. Note that all the dislocations were generated from the side surface of the sample and travelled a long distance into the crystal. Of particular interest in this sample are the dislocations that became curved between pinning points as they travelled (denoted by A in the Fig. 15(a)). Even nearly straight dislocations developed pinning points on moving, as in area

B of Fig. 15(a). The specimen was pulled again at 850°C under a resolved shear stress of ~ 36 gm/mm^2 with the hope of observing the continued motion of straight and curved dislocation lines in the same area and then the topograph (Fig. 15 (b)) was taken. There was no motion of either curved or straight dislocations. The applied stress was increased to a shear stress of ~65 gm/mm^2 and the specimen was pulled at ~900°C for 15 minutes. Figure 15(c) is the final topograph of the series. Intense multiplication of dislocations and formation of a band due to the movement of these curved dislocations occurred. The individual dislocations in the band could not be resolved since the dislocation density was too high (it is only possible to roughly estimate the density to be of the order of $\sim 10^6$ disl/cm^2). These bands could be the nucleating centres for slip bands.

E. Electron Microscopic Investigation

In as much as the resolution of the Lang technique is very poor, the present investigation was extended to study the nature of the dislocation substructure in deformed silicon by electron microscopy. When foils were made from lightly deformed samples and observed in the electron microscope, no dislocations or any other imperfections such as vacancy clusters, impurities or voids were found. Since the dislocation densities were less than 10^2-10^3 dislocation per cm^2 in lightly deformed specimens it is difficult to find them. However, few specimens were deformed under a tensile stress of ~200 gm/mm^2 along [110] at 920-950°C for 20 minutes to introduce dislocations of a density ~10^4 - 10^5 dislocations/cm^2. (The x-ray topograph shown in Fig. 15(c) probably corresponds to nearly this amount of deformation). The resulting electron micrographs are shown in Fig. 16(a) to (g). Of particular interest in this is the fact that some dislocations

are still smoothly curved at this magnification rather than angular but some segments are accurately straight. In some areas, bundles of long edge dislocation pairs or dipoles are seen (micrograph (a)), possibly left behind by the moving screw dislocations. Also in this micrograph are long loops, small loops and black dots of various sizes. A few dislocations change their directions abruptly (micrograph(b)). The micrograph (c) shows what may be a well developed large kink loop on a moving screw dislocation. However because only a single diffraction condition was used the possibility that these may be nodes cannot be ruled out; one of the three dislocations could be out of contrast. Straight as well as smoothly curved dislocations are present also in the micrograph (d), long loops and short segments of dislocations in (e) and smoothly curved and wavy dislocations in (h) and (g). Finally, dislocation dissociation was not readily observed in any micrograph, not even at the nodes in (a) and (g).

F. Motion of Individual Dislocations and Measurement of Dislocation Velocities

The main interest of the present investigation was to make unambiguous measurements of velocities of isolated dislocations at various temperatures under the same applied stress. A temperature range of 775°-925°C was found to be suitable for such studies for the following reasons. Temperatures above 900°C always lead to extensive climb of dislocations in addition to glide motion. Again, above 900°C dislocation generation from the side surfaces or edges of the sample was copious, thus filling the entire area of the specimen with many dislocations. On the otherhand, temperatures below 750°C were not suitable for making dislocations move appreciable distances in a reasonable amount of time, especially under the small applied

stresses that could be employed in the present investigation. The variation of dislocation velocities with applied stress was not investigated although such data would be extremely fruitful for the development of a reliable theoretical model. In our method of dead loading, a minimum of ten minutes of loading-time was impertive since it took at least three minutes for the specimens to attain the appropriate experimental temperature in the furnace. Under loads higher than 40 gm/mm^2, dislocation generation was profuse and the density increased rapidly with increase in loading time. Only under pulse-loading, would it be possible to study dislocation motion at higher stresses.

The first step was to find the optimum conditions to generate well isolated individual dislocations and then to study their continued motion under a stress that would not rapidly multiply dislocations in their vicinity As has been described previously dislocations introduced at about 1000°C by pressing a molybdenum pointer do not move at lower temperatures. When the pointer was pressed at about 800°C, the generated dislocations did not propagate far away from the point of compression and thus it was difficult to find areas containing isolated dislocations. The next approach was to deform the sample under tension at about 850°C, in the hope of introducing isolated dislocations. A resolved shear stress of 88 gm/mm^2 at 850°C. sometimes resulted in generating a few isolated dislocations. This experimental condition was realized by trail and error. Higher loads and higher deformation temperatures resulted in the introduction of dislocations in groups. The next problem was to find a small load to study the continued motion of the individual dislocations without causing multiplication of other dislocations in their vicinity. A resolved shear stress of 36 gm/mm^2 was just sufficient to move isolated dislocations enough to make velocity

measurements. A number of such experiments will now be described individually.

Figure 17 is the enlargement of topographs before and after tensile testing a specimen at 825°C under a resolved shear stress of 36 gm/mm^2. The geometry of the specimen and the loading direction are shown on the topograph itself. The velocities of screw and 60°- segments of many dislocations were measured and are listed in Table II. In the final column are given the characterisitics of the dislocation line, namely whether the dislocation was straight, wavy or curved. In particular, it was found that 60°- segments moved nearly 2 1/2 - 3 times faster than the screw segments. Also it was observed that some straight dislocations (No. 2,6,and 7) became either curved or wavy while some remained fairly straight (Nos. 5, 9 and 10). Dislocation segments lying ahead of a pile-up (Nos. 12, 13, 14, 15 and 16) moved at higher velocities as might be expected. Straight dislocations in general, moved at higher speeds than the curved ones (compare the dislocations No. 11 and 20 with No. 5 and 17). Conversely, dislocations moving at higher speeds remained straight, while slow-moving dislocations became wavy or curved. Instances were not uncommon where a long and straight dislocation moved to various extents at various parts of its length (see No. 4). Figure 18(a) and (b) contain the topographs of another specimen pulled in tension under a resolved shear stress of 36 gm/mm^{21} at 850°C. Again, the various dislocations are labelled and the data is listed in the Table III. Again the speeds of 60°- dislocations were higher than the screw segments by a factor of ~4. Of particular interest in this specimen is dislocation No. 1 that become wavy after moving. The motion of the dislocations Nos. 4, 5, 6, 7, and 8 were highly inhomogeneous and it was even difficult to measure unequivocally their velocities. The 60°- segments ahead of a pile-up (Nos. 13 and 14) travelled much longer distances than did the isolated

TABLE II.

Dislocation No.	Velocity in cm/sec $\times 10^{-5}$	Remarks
Screw Segments		
1	1.07	wavy; fairly uniform motion
2	2.14	straight; uniform motion, becomes wavy
3	~1.00	straight; not isolated, becomes curved
4.	1.34	straight; uniform motion, a portion is stuck
5	1.20	straight; uniform motion, be comes wavy
6	1.07	straight, non-uniform motion, becomes curved
7.	1.90,1.75	" " " " " "
8	1.15	not isloated, interacted by other dislocations in the group
9	2.27	straight, ahead of a pile-up
10	2.41	" " " " " "
11	~0.8	curved, resists motion.
60°-segments		
13	4.91	straight, moves uniformly becomes smoothly curved
14	4.80	straight, moves uniformly fairly retains straightness
15	3.75	straight, moves uniformly fairly retains straightness
16	3.80	straight, moves uniformly fairly retains straightness
17	4.53	smoothly curved, fairly uniform motion, retains shape
18	4.05	highly irregular motion, becomes curved
19	4.42	fairly uniform motion
20	3.50	irregular motion, not isolated, ahead of a pile-up
21	5.15	smoothly curved, well isolated

TABLE III

Dislocation No.	Velocity in cm/sec $\times 10^{-5}$	Remarks
Screw Segments		
1	2.14	straight, fairly uniform motion, becomes wavy
2	2.60	straight, ahead of a pile-up.
3	1.36	piece wise straight, irregular motion
4,4'	3.21	straight, non-uniform motion, becomes irregular
5	2.91	straight, non-uniform motion, becomes irregular
6,6'	2.94, 3.3	straight, non-uniform motion, becomes irregular
7,7'	2.43	straight, non-uniform motion, becomes irregular
8	1.09	straight, non-uniform motion, becomes irregular
10	1.61	straight, fairly uniform motion, becomes curved
13	3.10	not isolated, ahead of a pile-up
60°- Segments		
1	8.0	straight, becomes smoothly curved
2	7.48	curved, non-uniform motion
4,4'	6.14, 6.95	smoothly curved, uniform motion
5	5.73	smoothly curved, uniform motion
6	3.21	smoothly curved, uniform motion
9	9.35, (1.07×10^{-4})	non uniform motion
13	9.4, (1.1×10^{-4})	straight ahead of a pile-up, retains its shape

segments and these high speed segments also remained straight after moving. Figures 18(c) and (d) show topographs of the above specimen after continuing the tensile testing at 800° and 775°C respectively. The general features regarding dislocation motion are the same as described earlier. Of particular interest in these topographs are the dislocations that straightened out on pulling at 775°C (Compare the Figs. 18(c) and (d) and observe the dislocation lines Nos. 4, 10, 14 etc.). This straightening and aligning along the low index planes is not an isolated case but quite general. Velocities of various dislocations at 800° and 775°C were measured from these topographs. Figures 19(b) and (c) shows the topographs of a specimen loaded at 900° and 920°C respectively. The glide plane for the dislocations, shown in Fig. 19(a), is steeply inclined to the surface of the specimen (see the geometry of the specimen shown on the topograph itself). Thus, the distances travelled by the screw segments are more unfavorable for measurement than in the previous specimens. In Fig. 19(a) and (b), dislocation motions were fairly uniform. The 60°- segments moved with a velocity 3-4 times that of the screws. In Fig. 19(c), motion of dislocations at 920°C is shown.

To summarize the observations in the foregoing paragraph: dislocation velocities were not very uniform, straight dislocations became wavy or curved immediately after they started moving, isolated straight dislocation lines moved more uniformly with a constant velocity. Some segments became immobile soon after moving a small distance and resisted motion when the test was continued at other temperatures. Such segments were only a few and seen at random, indicating that the effect may be due to impurities.

The velocity data for screw and 60°- dislocations are displayed in Figs. 20 and 21. The logarithm of velocity is plotted against the reciprocal

of absolute temperature. Straight lines were drawn through the data points and their slopes were determined by a least square best fit method. The apparent activation energies for the dislocation motion were calculated from these slopes. This gave a value of 1.8 ± 0.3 e.v. for screw as well as 60°- dislocations.

IV. DISCUSSION

A. Nucleation and Generation of Dislocations

When specimens with nearly zero inital dislocation densities were deformed in tension, groups of like dislocations were generated from sharp corners or surfaces. Suzuki and Kojima[15] found in their samples (of purity comparable to ours) that dislocations were nucleated from some unknown centres where no particular images were found prior to deformation. They attributed this to some unresolvable impurity clusters, presumably oxygen impurities, but could not pursue the question further due to the limitation of the technique. The present investigation clearly shows that dislocations were not nucleated at random throughout the sample, rather, many were generated from the surface. In samples which were smoothly polished and subsequently handled with care, it was more difficult to nucleate dislocations. This clearly shows that mechanical stress raisers such as sharp corners or surfaces with locally deformed areas or oxide-films are responsible for the generation of dislocations. A few samples were quenched from temperatures very near to the melting point, and subsequently aged at 1000°C to condense vacancy-clusters, voids or loops; it was found that dislocation generation in these samples was more difficult. Voids or vacancy clusters did not act as sources for dislocations but were found to be obstacles for the passage of dislocations. Nor did we find in any samples old dislocations acting as sources. Thus, the present work shows that pre-existing dislocations or vacancy-clusters or voids do not act as sources for dislocations in the initial stages of plastic deformation.

The pressing of a molybdenum pointer on the surface of the specimen, used in the present work to generate dislocations, is similar to a hardness

indentation. The resulting dislocation configuration was groups of dislocations generated near the point of compression, approximately lying along ⟨110⟩. None of them were exactly straight or angular but were smoothly curved. If kink nucleation is the rate controlling process for dislocation motion, one would expect dislocations to remain straight and align along the low index planes. Therefore, this does not seem to be the most important barrier to dislocation motion at 1000°C. Many cusps and pinning points on the dislocation line, like the examples of Figs. 5, 6 and 7, suggest that dislocations are heavily jogged. The rate controlling process might be the non-conservation motion of jogs on dislocations which are near screw orientation.

It can also be observed in Figs. 5 and 6 that screw segments of all dislocation lines are longer than the 60°- segments by a factor of 4 to 5. Although individual dislocations adjacent to the point of compression are not well resolved in the topographs, close observation reveals that this is true even for the inner-most loops. If the velocity stress dependence is assumed to be roughtly the same for a dislocation of any orientation (i.e. edge, screwof mixed), one would expect the inner most loops to be roughly circular. Thus it appears that the velocities of screw and 60°- segments are intrinsically different right from the time they are emitted by the source. If the dislocation line is jogged at high temperature, one could account for the slower motion of screw segments when compared to 60°- segments. Since the jogs on screws have to be dragged non-conservatively along the dislocation, they exert a much larger dragging force on the screws than on edges or 60°- dislocations.

B. Propagation of Dislocations at High Temperatures

The present work clearly shows that dislocations near screw orienta-

tion developed pinning points, dipoles and even large loops as they moved in the crystal at about 1000°C. This can be explained by assuming that moving screw dislocations continuously develop jogs at high temperatures.[22] Consider a long screw dislocation having jogs of varying sizes (see Fig. 22). Continued motion of the dislocation will result in the formation of a long dipole if the jog is at least several burger's vector high but the unit jogs can be dragged along leaving behind a trail of vacancies or interstitials depending upon the sign of the jog. If the jog height exceeds the distance given by

$$h = \frac{\mu b}{8\pi(1-\nu)\tau} \qquad (1)$$

where τ is the shear-stress acting on the dislocation line and other symbols have the usual meaning, then the two edge segments of the dipole can be driven past each other in the opposite direction by the applied stress. The resulting configuration is a cross-over loop. One can identify all these features on the moving dislocation line in Fig. 12(a).

Although jogs on moving screw dislocations large enough to result in dipole trails have been observed by many investigators, it is not clearly established how the jogs were introduced initially on the moving screw dislocation. Jogs of appreciable size can be introduced by a number of mechanisms.[22] An obvious process is intersection of two dislocations resulting in either acquisition of jogs by both the dislocations or a jog by one dislocation and kink by the other. The moving screw dislocation can also acquire multiple jogs if it cuts a grown-in small angle twist boundary or a group of dislocations. Double cross-slip or a combination of cross-slip and climb can also lead to jog formation under certain conditions. Even impurity clisters, fine precipitates or voids could cause local double cross-slip due to their

stress fields. It is extremely difficult to know which of these mechanisms are most important in a given situation.

In the present work, the intersection mechanism can be ruled out on the grounds that the crystals were dislocation free and there were no small angle boundaries or grown-in dislocation net work. Similarly, there was no evidence for the presence of impurity clusters or precipitates. But, it is proposed that climb of a short sequent of a nearly screw dislocation could lead to jog formation as follows:

Consider a long screw dislocation moving on the primary glide plane that is pinned at its ends by a small dipole (see Fig. 23). When the dislocation attempts to move further, the segment between the pinning points bows out. The mid-point of the bowed out segment is exactly in pure screw, while the segments just to the left and right of the mid-point are very nearly of screw orientation with the edge part of the left side having the extra half plane above the glide plane and that of the right side below the plane. If excess vacancies around the dislocation cause the climb of the edge component, the left and right sides will climb in opposite directions. Any additional movement of the dislocation is accompanied either by dragging of the jogs non-conservatively or if the jog is of sufficient height, an edge dislocation pair will be formed. The spacings of the dislocation pair can increase by the addition of more vacancies which the moving dislocation collects while sweeping the glide plane. Vacancies can arrive at the dipoles by diffusing along the dislocation line (pipe-diffusion). Similarly, new jogs can glide into the growing dislocation pairs, thus increasing (or decreasing) their separation.

Vacancies in excess of equilibrium concentration could be present in the crystal due to the dragging of some small jogs non-conservatively by the moving dislocations. Large voids and vacancy clusters could also have

been left in the lattice during the growth of the crystal from the liquid state. Voids in silicon samples grown from the liquid state is a hydrogen atmosphere has been reported by Yukimoto[23]. Vacancies can also be trapped in the crystal while cooling from high temperatures.*

An electron microscopic investigation has been undertaken in an attempt to determine whether or not any voids were present in the silicon samples used in these experiments. Since the density of such vacancy-clusters must be extremely low it becomes difficult to find them in an electron microscope thin foil.

C. Effect of Aging on Dislocation Mobilities

The experimental results described previously also show that dislocations generated at high temperatures (~ 1000°C) or exposed to high temperatures, become immobile at lower temperatures (~ 850°C) even under loads high enough to generate and move fresh dislocations (see Fig. 10). The effect is quite general and extends over the whole length of the dislocation line. If the applied stress is increased in steps, a critical value is reached when catastrophic multiplication occurs (see Fig. 15). We know that movement of jogged dislocations could result in multiplication. (This point will be further discussed in the next section). As has been discussed earlier, non-conservative motion of jogs on screws also produce large drag stresses. Therefore it is possible that dislocations are immobilized during aging by becoming heavily jogged. After heating to high temperatures all pre-

---

*Tweet's[24] experiment in germanium is of particular interest in this connection. When dislocation free germanium crystals were cooled fast from high temperature, they etched unusually rapidly. If the samples were cooled very slowly taking care not to retain any vacancies in the crystal, the anomalous etching disappeared. When crystals with dislocations in them were quenched first from high temperature, etching was not rapid in the regions surrounding the screw dislocations because they were absorbed and screw dislocations climbed into helices.

existing dislocations could become jogged by climb as discussed in the previous section. It is not possible to ascertain from the present investigation whether or not dislocations are also locked during aging by impurities or impurity clusters. Impurities could cause the screw dislocations to double cross-slip due to elastic interactions, thus contributing to jogging of the dislocation. Such a mechanism has been originally put forward by Johnston[25] to account for the dragging stresses on screw dislocations due to the presence of small amounts of impurities. A combination of impurity pinning and dislocation climb may be even more effective in immobilizing the dislocation at high temperature. It is possible that whenever a dislocation spends time due to pinning in a fixed position or moves very slowly localized climb may generate jogs of considerable height. The existing experimental data is still too sparse to confirm which of these mechanisms is important. It is not likely that x-ray topography can contribute directly to answering these questions because of the limited resolving power.

D. Electron Microscopic Investigation

The present electron microscope results on the nature of dislocations in silicon lend support to similar observations made on deformed germanium by Alexander and Haasen[26]. Although the present work is limited, the following salient features emerged from the study of the micrographs. The observed configurations were mainly edge dislocation dipoles and elongated loops of varying lengths and widths, apparently left behind by moving screw dislocation. Free individual dislocations were rarely found in the primary slip plane. Those dislocations that were observed were relatively immobile and did not move even under prolonged beam heating. Further, the

dislocation distribution was highly inhomogeneous. Large areas were free of dislocations while clusters of entangled dislocations were distributed on the primary slip plane. Three dimensional dislocation tangles were not observed. These observations are not only similar to those made on germanium but also are like those on copper[27] during stage I of deformation. We did not observe any cross-slipping in the present electron microscopic work, but Alexander and Haasen[26] reported that screw dislocations did move in the cross-slip plane in their germanium samples, (deformed under a stress of ~ $1 kgm/mm^2$).

The localization of deformation into the narrow regions on the primary slip plane can only be explained by the avalanche-like multiplication due to individual dislocation sources. The dipole formation mechanism as proposed by Washburn[21] and the cross-over dipole sources as observed in silicon-iron by Low and Turkalo[27] can explain most of the present observations. As has been pointed out in earlier section, the configuration resulting from the movement of jogged screw dislocations depends on the size of the jogs. We have proposed a possible mechanism for the formation of a jog of several burgers vectors due to the climb of a short segment of a nearly screw dislocation. It is possible to extend this mechanism to show how closed dipole loops can be formed by continued motion of the dislocation line. If new jogs are formed on the bowing segments on either side of the cusps, they can glide into the growing dipole conservatively. If the number of jogs of opposite sign that run into the dipoles become equal, then the loops can be terminated. For very large jogs, the spacing between the edge dislocation pairs will be enough to permit the applied stress to overcome their mutual attraction and they can move independently of each other. This type of cross-over seems to be the source for dislocation multiplication in

silicon at high temperatures. The stability of dipoles depends upon their heights and the applied stress. Therefore, when the applied stress increases, previously immobile dipoles become dislocation sources.

E. Mobilities of Individual Dislocations

It is well known that the velocity of a dislocation under a given stress and temperature depends upon a number of factors such as its orientation, its radius of curvature, its interaction with other dislocations, amount and the types of impurities, the resistance offered by the crystal lattice itself etc. A theoretical estimation of resistance to motion due to all these factors is very difficult. Although experimental evidence on the speeds with which dislocation travel during plastic deformation is available, quantitative information on dislocation velocity as affected by the above factors is lacking. In the present investigation, speeds of dislocations were measured and the data has been correlated with the general appearance and the geometry of the dislocation lines.

1. Pinning of Moving Dislocations

The most striking observation common to all the moving dislocations was that they become wavy or curved almost immediately after they started moving. A close observation of a moving dislocation, as for example dislocation number 1 in Fig.18, reveals a number of pinning points along its length. Some dislocations become smoothly curved while some others assumed highly irregular shapes. Dislocations which were ahead of a pile-up moved with much higher velocities and retained their over-all straightness more readily compared to the isolated ones. The portion of the dislocation where it changed from screw- to 60°- orientation loses its angularity and becomes smoothly curved. 60°- dislocations moved invariably faster than

the screws by a factor of 4 or 5 and the pinning points on them were less pronounced. They also retained their straightness more than the screws.

The pinning points on the dislocation line must be associated either with vacancy clusters and impurities or with thermal jogs. The poor resolution of the present technique does not make it possible to decide definitely which of these two possibilities is most important. When a dislocation line interacts with impurities as it slowly moves on the glide plane, individual segments pinned by impurities at their ends will bow-out to different amounts depending on their free lengths and the local shear-stress acting on them. This will make the dislocation appear as wavy or curved. Similarly jogs on screw dislocations act as dragging points since they cannot move along with the dislocation line conservatively. This will also cause the advancing dislocation line to bow-out in between the dragging jogs. Certain of the experimental observations suggest that jog-pinning is more appropriate in the present case than the impurity-pinning. For example, the pinning points are more or less uniformly distributed along the entire length of the dislocation line. As will be discussed in the following paragraphs, the average pinning distance decreases with increasing temperature. The pinning points are present on all dislocations without exception although the effect is less prnounced on dislocations moving with slightly higher velocities, as those ahead of a pile-up or near the edge of the specimen. When few individual dislocations were originally generated from the edges of the specimen, they were accurately straight. (See the dislocations No. 2, 4, 5, 6, and 7 in Fig. 17(a) and Nos. 1, 4, 5, 7 in Fig. 18(a).) They became wavy or curved after moving on the glide plane under the applied stress. If impurities were responsible for pinning, the effect should be more random and should vary from specimens to specimens. The present

observations are contrary to this.

It is not possible to measure the pinning distances unambiguously since the pinning points are not sharp and well-defined. However an attempt was made and the results are displayed in Fig. 24. In this figure, the logarithm of pinning distances are plotted against the reciprocal of the temperature. The manner in which the pinning distances are arrived is as follows: The dislocation line was closely observed under a magnification of 40× in a metallographic microscope* and the distances between the cusps were measured as closely as possible. The smallest distance that could be measured with reproducibility was ~ 20μ. If these pinning points are attributed to thermal jogs, the dislocation line will contain about equal number of jogs of both sign**. The distances between the cusps were measured several times and an average value was taken for each temperature.

As shown by Friedel[28], the equilibrium length ℓ_j between unit high jogs on a screw dislocation should be given by

$$\ell_j = b\, e^{u_j/kT} \qquad (2)$$

where u_j is the jog energy and other symbols have their usual meaning. From the slope of the line in Fig. 24 a value of 1.1 - 1.2e-v is obtained for jog energy. In covalent metals such as silicon, this is not a too unreasonable value.

---

*The pinning points on the dislocation line, say No. 1 in the Fig. 18(b), can be more easily recongized by holding the print at the eye level and viewing the dislocation line along its length.

**The two types of jogs referred here are vacancy-jogs and interstitial-jogs. Except at very high stresses, the interstitial jogs move by absorbing vacancies rather than by creating interstitials since the latter have usually very high energy of formation.

2. Thermally Activated Process

When a moving screw dislocation is pinned by jogs, its mobility is greatly impeded. Under an applied stress τ, the dislocation line bows-out between the pinning points and takes a form similar to that of Fig. 25. Geometrically, such a bow-out corresponds to the pile-up of kinks of opposite sign on opposite sides of the pinning points.[29] The jogs can move forward only by climb. Thus, under applied stress τ, the glide of a bowed screw dislocation must involve both the generation and propagation of kinks and the nonconservative motion of jog. Therefore, it is necessary to distinguish which of the two, namely either kink-nucleation and propagation or climb of jogs, is the rate-controlling process for the dislocation glide in the present case.

Let us first consider the case of the climb of jogs on screw dislocations. Referring to Fig. 5, the force F acting on jogs due to the line tension is given by

$$F = 2\Gamma \cos\frac{\alpha-\theta}{2} = 2\Gamma\left[\cos\frac{\alpha}{2}\cos\frac{\theta}{2} + \sin\frac{\alpha}{2}\sin\frac{\theta}{2}\right] \qquad (3)$$

where θ is the radius of curvature of the dislocation line and Γ is the line tension. From the topographs, it was very difficult to measure the angle α as a function of temperature, since the scatter was high and the reproducibility was poor. Close observation suggests that α does not vary very much with temperature. That is, the dislocation line on the either side of the jogs has to bow-out to a certain critical curvature, irrespective of temperature, before the jogs can advance in the forward direction. This strongly suggests that the jogs were moving forward without the aid of thermal fluctuations. Another factor that was not unambiguously clear from the

topographs is the radius of curvature of the segments themselves. Two bowed out configurations are possible. The entire segment of the dislocation line pinned by the jogs can bow-out with a uniform equilibrium radius of curvature. The second possibility is that the middle part of the segment, is almost straight and only the portions of the segments on either side of the jogs are curved. From the topographs, it was not evident which of these two configurations is appropriate in the present case. This is again due to the poor resolution of the technique. The dislocation images, when observed at magnifications higher than 40× were diffuse and lower magnifications increase uncertainties and errors in the measured values. The image widths were also not favorable to quantitative measurements. Qualitative observations (especially topographs of specimens which were treated at lower temperatures) show that the dislocation was more sharply curved near the jogs leaving the middle portions of the segment relatively straight. This is consistent with the idea that the dislocation advances by nucleation of kink-pairs and their subsequent slow sidewise motion towards the pinning jogs. When a critical radius of curvature is reached on both sides of the jogs due to kink pile-ups, the jogs move forward athermally. If the entire bowed-out configuration of the dislocation line advances a distance b per emission or absorption of a single vacancy by jogs, the work produced by the applied stress τ is $\tau b^2 \ell_j$. For an average value of ℓ_j=20μ and τ=36gm/mm^2, this work becomes ~7 e.v. Since this is very large, the jogs can advance by this purely mechanical process leaving behind rows of point defects. This very large work done by the applied stress is due to the large distances between jogs. Therefore, it is concluded that in the present case, jogs on screw dislocations do not control their glide motion; but do account for the general appearance and the shape of the moving dis-

location lines.

As shown by Friedel[28], if the Peierls Nabarro force σ_{PN} is larger on jogs than on the rest of the dislocation line segments will bow-out between jogs to an equilibrium configuration governed by the equation

$$\sigma_{PN} = \mu b^2 \sin(\psi + \frac{\alpha}{2}) + \sin(\psi - \frac{\alpha}{2}) \qquad (4)$$

For α smaller than a critical value, the jogs will be able to glide in the direction of burger's vector as shown in Fig 26. Thus, for dislocations which are in 60°- orientation and for those portions between screw to 60°- orientation, the jog motion may be conservative. This could explain the greater smoothness of dislocations in this orientation. (As stated earlier, the pinning points on these dislocations were less pronounced).

3. Activation Energy for Glide Motion

According to the above interpretation, the thermally activated process of dislocation motion is identified with the nucleation of a pair of kinks and their subsequent propagation along the dislocation line. Dislocation velocities in silicon and germanium as a function of applied stress and temperature have been measured by Chaudhuri et. al.[3], Haasen[5] and Kabler[4] by the etch-pit technique and by Suzuki and Kojima[15] by x-ray topographic technique. From the temperature dependence, activation energies were estimated by these workers by characterising the dislocation motion as a simple thermally activated process. Chaudhuri et. al. obtained a value of 2.2 e.v. for silicon. This energy was found to be 2.4 ± 0.2 e.v. by Suzuki and Kojima[15]. This energy was identified with the work required to form a pair of kinks of a critical separation above which the kinks can move apart along the dislocation line under the action of the applied stress. Theoretical calculations of the peierls force and hence the activation

energy required to move a dislocation by forming kink-pairs has been done by Celli,[31] Suzuki[32] and Labusch[33] and these are given in Table IV. The experimental results of the previous authors are in excellent agreement with these theoretical estimates.

Although the above results suggest that for gross dislocation movement kink nucleation is probably the rate controlling process, Southgate and Attard[30] interpreted their internal friction data in silicon in terms of the "Peierl's energy of a second kind" as originally suggested by Brailsford[29]. In this model, kinks on dislocations are taken as abrupt and their movement along the dislocation line is considered to be thermally activated. A straight dislocation pinned at two ends contain uniformly spaced kinks, so that, on the average it takes the shortest path. Transport equations were formulated for the motion of kinks along the dislocation line. Southgate and Attard obtained a value of 1.61 ± 0.05 e.v. for the activation energy from their interval friction data. This energy was identified with the energy required for motion and redistribution of kinks under the applied stress, which was thought to be responsible for the dislocation damping. Since bond energies in silicon is approximately 1.82 e.v., they concluded that kink propagation along the dislocation line involves breaking of bonds.

As has been discussed earlier, the present observations on moving dislocations show that they are not straight; only their general direction is along the low index planes. The geometrical shapes of the dislocations observed in the present experiments vary from smoothly curved to highly irregular. If only the kink nucleation process is difficult and kink migration velocity is high, one would expect the dislocation lines to be more rectilinear than the presently observed irregular geometry. Therefore, in the following, the glide of the dislocations line will be formulated in

TABLE IV

Author	Peierl's energy ev/cm	Energy to nucleate a kink - pair (e.v.)
Celli	3.8×10^6	2.02
Suzuki	13.1×10^6	2.30
Labusch	6.9×10^6	2.14

terms of thermally activated process of kink-pair nucleation and migration.

The formulation of the Peierl's mechnism of dislocation motion has been worked out by a number of workers assuming varying mathematical models for kink nucleation and propagation. This is mainly because there as yet no general model that is applicable to all crystalline materials. In the Appendix, the kinetic equations for kink nucleation and migration are written down appropriate to our case, following the formulation of Dorn and Rajnak[34]. The forward velocity of the dislocation line has been shown to be (see Appendix)

$$v = \frac{4\nu b}{\pi}\left(\frac{\tau_p \tau b^3}{\mu k_T}\right)^{1/2} e^{-\frac{E_m + E_n(\tau)}{2 k_T}} \qquad (13)$$

It can be seen from this expression that a plot of $(\ell n\, v + \frac{1}{2}\, \ell n\, kT)$ against $\frac{1}{T}$ will yield the activation energy. This is done in Fig. 27 for screw dislocations. From the slopes, the activation energies are estimated as 1.78 e.v. for the upper curve and 1.75 e.v. for the lower curve. It will be of interest to derive the velocity-stress law from Eq. 13. This can be done by examining the pre-expomential term. As stated in the Appendix, E_n is a function of applied stress. As shown by Dorn and Rajnak the quantity E_n/E^*, where E^* is the energy required to nucleate a pair of kinks under zero stress (in other words, E^* is the kink-nucleation energy), depends only upon $\frac{\tau}{\tau_p}$. Thus, $\frac{E_n}{E^*}$ vs $\frac{\tau}{\tau_p}$ curves are universal relationships. For very small values of $\frac{\tau}{\tau_p}$, as is the present case, their plots yield

$$E_n = E^* \left\{1 - \frac{\tau}{\tau_p}\right\}^{3/2} \qquad (14)$$

The pre-exponential term in the velocity equation also involves τ_p. For the upper line in Fig. 30, the measured pre-exponential value is $\sim 8.82 \times 10^2$ cm - e.v.$^{1/2}$/sec. By equating this to the pre-exponential

term in equation, one obtains τ_p to be ~1.76×10^{10} dynes/cm^2. By itself this value has no significance at all, since τ_p will depend upon the assumed shape of the potential. Even so, this result shows that the term $\frac{\tau}{\tau_p}$ is extremely small for stresses of the order of 40 gm/mm^2. Therefore, the exptential

$$e^{-E_n(\tau)/kT} = e^{\frac{-E^*(1-\frac{\tau}{\tau_p})^{3/2}}{kT}}$$

can be approximated, by Taylor series and power series expansion, as

$$e^{-\frac{E^*(1-\frac{\tau}{\tau_p})^{3/2}}{kT}} \simeq \frac{3}{2}\left(\frac{\tau}{\tau_p}\right) e^{-E^*/kT}$$

Hence, for small applied stresses, the velocity Eq. 13 becomes

$$v = \frac{4\nu b}{\pi}\left(\frac{\tau_p \tau b^3}{\mu kT}\right)^{1/2}\left(\frac{3}{2}\frac{\tau}{\tau_p}\right)^{3/2} e^{-\frac{(E^* + E_m)}{2kT}}$$

This equation shows that the velocity-stress relationship is of the form $v \alpha \tau^{2.0}$, identical to the observed relationships in silicon and germanium by previous workers.

V. CONCLUSIONS

The present experimental observation and subsequent discussion lead to the following conclusions:

1. In highly perfect silicon crystals with nearly zero initial dislocation density, generation of dislocations took place at or near the surfaces. Vacancy clusters or loops did not act as dislocation sources; but were obstacles to the passage of dislocations.

2. Dislocations generated at high temperatures (~1000°C) were immobile at lower temperatures (~ 850°C). This was attributed to the jogging of dislocations at high temperatures possibly by climb.

3. Above a critical stress that is dependent on the deformation temperature, motion of dislocations results in the catastrophic multiplication of dislocations. The detailed configuration of such dislocation bands, studied by transmission electron microscopy, consists of opposite dislocation pairs or dipoles, narrowly distributed on the main slip plane. These observations are explained in terms of the dipole formation mechanism of Washburn.

4. From the detailed study of the appearance or shape of moving dislocations, a value for the activation energy for jog formation was roughly estimated to be ~1.2 e.v.

5. Values of the apparent activation energy for the glide motion of screw and 60°- dislocations were found to be 1.8 ± 0.3 e.v. at a stress of ~36gm/mm^2. This energy is identified with the average of the sum of the energies required for kink-pair nucleation and migration.

6. A study of the pre-exponential term from the velocity vs reciprocal temperature indicates the stress dependence of velocity as $v \sim \tau^2$.

ACKNOWLEDGEMENTS

The author is deeply grateful to Professor Jack Washburn for his guidance, encouragement and advice throughout this investigation. My special thanks are also due to Professor John Dorn for several stimulating discussions, Dr. Bernard Escaig for many helpful comments, Mr. George M. Gordon for his assistance in the x-ray laboratory and Jane Ball for her special efforts in typing this thesis.

This work was done under the auspices of the United States Atomic Energy Commission through the Inorganic Materials Research Division of the Lawrence Radiation Laboratory.

APPENDIX

Following the formulation of Dorn and Rajnak, we will set up kinetic equations for kink nucleation and migration, appropriate to the present case, assuming simple-minded models for the reaction rates. Consider a long dislocation line moving under an applied stress by nucleation of a pair of kinks and subsequent sidewise motion of kinks along the dislocation line (see Fig. 28). The frequency ν_n of nucleation of pair of kinks per unit time in a length ℓ is

$$\nu_n = \nu\left(\frac{b}{w}\right)\frac{\ell}{2w}\, e^{-E_n(\tau)/kT} \tag{5}$$

according to the Boltzmann condition, where $E_n(\tau)$ is the energy required to nucleate a pair of kinks, which essentially depends upon the applied stress, ν is the Debye frequency and w is the critical width of the kink-pair and other symbols have their usual meaning. Similarly, the kink velocity is given by

$$v_K = \nu\, b\, e^{-E_m/kT} \tag{6}$$

where E_m is the activation energy for the migration of kinks. The lateral force component on the kink due to an applied stress τ is τb^2. Therefore, for the case of sidewise migration of kink pairs under a stress τ, Eq. 6 becomes

$$\begin{aligned} v_K &= \nu b \left\{ e^{-\frac{(E_m - \tau b^3)}{kT}} - e^{-\frac{(E_m + \tau b^3)}{kT}} \right\} \\ &= 2\nu\, b\, e^{-E_m/kT} \sinh \frac{\tau b^3}{kT} \end{aligned} \tag{7}$$

For small values of τ, the hyperbolic function can be replaced by $\frac{\tau b^3}{kT}$ itself i.e.

$$v_K = 2\nu b \quad e^{-E_m/kT} \quad \frac{\tau b^3}{kT} \tag{8}$$

Let us assume that the average distance of the sidewise motion of a kink-pair before annihilation is (see Fig. 28) neglecting any acceleration effects, given by

$$\ell_m = \frac{2v_K}{\nu_a} \tag{9}$$

where ν_a is the frequency of annihilation of kinks. When the steady state is attained, the frequency of annihilation will be equal to the frequency of nucleation of kink-pair in length ℓ_m. That is

$$\ell_m = \frac{2v_K \, 2w^2}{\nu b \; \ell_m} \quad e^{E_n(\tau)/kT}$$

or

$$\ell_m^2 = 8w^2 \quad e^{-E_m/kT} \quad e^{E_n(\tau)/kT} \quad \frac{\tau b^3}{kT} \tag{10}$$

The average forward velocity v is given by

$$v = \nu_n \, b = \frac{\nu b^2}{2w} \quad \ell_m \quad e^{-E_n(\tau)/kT}$$

or

$$v = \frac{2\nu b^2}{w} \quad \left(\frac{\tau b^3}{kT}\right)^{1/2} \quad e^{-\frac{E_m + E_n(\tau)}{2\,kT}} \tag{11}$$

The kink-width w varies very slowly with applied stress. For "quasi-parabolic" Peierls' hills[35], w is given in terms of the Peierl's stress τ_p as

$$w = \frac{\pi b}{2} \quad \left(\frac{\mu}{\tau_p}\right)^{1/2} \tag{12}$$

substituting this in the velocity equation, one obtains

$$v = \frac{4\nu b}{\pi} \left(\frac{\tau_p \quad \tau b^3}{\mu kT}\right)^{1/2} \quad e^{-\frac{E_m + E_n(\tau)}{2kT}} \tag{13}$$

REFERENCES

1. W. G. Johnston and J. J. Gilman, J. Appl. Phys. 30, 129 (1959).
2. D. F. Stein and J. R. Low, J. Appl. Phys. 31, 362 (1960).
3. A. R. Chaudhuri, J. R. Patel and L. G. Rubin, J. Appl. Phys. 33 , 273b (1962).
4. M. N. Kabler Phys. Rev. 131, 54 (1963).
5. P. Haasen, Disc. Faraday Soc. 38, 191 (1964).
6. K. Marukawa, J. Phys. Soc: of Japan, 22, No. 2, 499 (1967).
7. H. W. Schadler, Acta Met. 12, 861 (1964).
8. R. W. Rhode and C. H. Pitt, J. Appl. Phys. 38, 876 (1967).
9. W. F. Greenman, T. Vreeland Jr. and D. S. Wood, J. Appl. Phys. 38, 3595 (1967).
10. H. L. Prekel and H. Conrad, pp. 131, Dislocation Dynamics, edited by A. R. Rosenfield, Y. T. Hahn, A. L. Bement Jr., R. I. Jaffee, McGraw-Hill.
11. F. W. Young, Jr, and F. A. Sherrill, Can. J. Phys. 45, 757 (1967).
12. P. Petroff and J. Washburn, J. Appl. Phys. 37, 4987 (1966).
13. Theory of crystal dislocations by F. R. N. Nabarro, Clarendon Press (1967).
14. F. R. N. Nabarro, Z. S. Basinski and D. B. Holt, Adv. in Phys. 13, 193 (1964).
15. T. Suzuki and H. Kojima, Acta Met. 14, 913 (1966).
16. V. Celli, M. N. Kabler, T. Ninomiya and R. Thompson, Phys. Rev. 131, 58 (1963).
17. E. S. Meieran and K. E. Lemons, Adv. in X-ray Analysis, 8, 48(1964).

18. A. R. Lang, Encyclopedia of X-rays and V-rays (Reinhold pulbishing co. New York) 1963.

19. B. W. Batterman and H. Cole, Rev. Mod. Phys. 36, 681 (1964).

20. W. W. Webb, Direct Observation of Imperfections in Crystals (Interscience Publication, New York, 1962) pp. 29.

21. J. E. Lawrence and H. Koehler, Jour. of Sci. Instruments, 42, 270 (1965).

22. J. Washburn, Electron Microscopy and the Strength of Crystals, G. Thomas and J. Washburn, editors, Interscience Publ., New York (1963), Chapter 6.

23. Y. Yukimoto, Jap. J. Appl. Phys. 7, 348 (1968).

24. A. G. Tweet, J. Appl. Phys. 29, 1520 (1958).

25. W. G. Johnston, J. Appl. Phys. 33, 2050 (1962).

26. H. Alexander and P. Haasen Can. J. Phys. 45, 1209 (1967).

27. J. R. Low and A. M. Turkalo, Acta. Met. 10, 215 (1962).

28. J. Friedel, Dislocations, Addison-Wesley Pub. (1964).

29. A. D. Brailsford, Phys. Rev. 122, 778 (1961).

30. P. D. Southgate and A. E. Attard, J. Appl. Phys. 34, 855 (1963).

31. V. Celli, J. Phys. Chem. Solids 19. 100 (1961).

32. H. Suzuki, J. Phys. Soci. Japan 18, Suppl I 182 (1963).

33. R. Labusch, Phys. Stat. Sol. 10, 645 (1965).

34. J. E. Dorn and S. Rajnak, Transaction of AIME 230, 1052 (1964).

35. P. Guyot and J. E. Dorn, Can. J. of Phys. 45, 983 (1967).

FIGURE CAPTIONS

Fig. 1. Diagram showing the dimensions of the tensile sample.

Fig. 2. A topograph showing dislocations generated by a molybdenum pointer on the surface of the sample at 1100°C for 30 minutes. Note the multiplication of dislocations very near to the point of compression. Observe long screw dislocations at (A) ($\bar{b} = \frac{a}{2}[\bar{1}01]$), showing presence of pinning points on them.

Fig. 3. Sketch of the experimental arrangement explaining the principles of Lang technique for taking topographs.

Fig. 4. Lang camera with the Hilger Microfocus x-ray tube. To limit the vertical divergence, a psuedo-focus source (1 × 1.4mm dia source seen end-on) was used. A take-off angle of 6 gives the best intensity and resolution.

Fig. 5. Dislocations generated by the molybdenum pointer in an initially dislocation free crystal. The temperature of deformation was 1000°C. Observe extensive cross-slip of long screw dislocations at A. (a) and (b) are $\bar{1}\bar{1}1$ and $1\bar{1}0$ topographs respectively.

Fig. 6. Dislocations generated by pressing the molybdenum pointer at 1025°C for 15 minutes. (a) and (b) are $\bar{1}\bar{1}1$ and 011 topographs respectively. The specimen orientation was not a low-index plane.

NOTE: The solid black line shown in the topographs in Figs. 2 and 5 through 14 is 2mm long, while in Figs. 15 and 17 through 19 is 1 mm long. In all the electron micrographs (Fig. 16), the solid line represents 0.5μ .

Fig. 7. Long screw dislocations generated by pressing a molybdenum pointer at high temperatures. Observe small pinning points (A), cusps (b) and cross-over loops (C) on the moving dislocations.

Fig. 8. Generation and propagation of dislocations at 1025°C by molybdenum pointer. The well isolated long dislocations at A are nearly in screw orientation. The line No. 1 shows presence of pinning points along the length of the dislocation, while No. 2 is smoothly curved. Large cross-over loops can be seen at (B), small cross-over loops at (C) and well developed cusps at (D).

Fig. 9. Annealing of dislocations at 1050°C without load for 30 minutes a), b) and c) are topographs before annealing and d), e) and f) are topographs after annealing.

Fig.10. Tensile deformation (stress = 88gm/mm^2 along [$\bar{1}$10]) of a sample at 825°C with previously introduced dislocations at high temperatures (~1000°C). The high temperature dislocations did not move (compare (a) and (b)). On pulling under higher-stresses (330gm/mm^2 along [$\bar{1}$10]) at 825°C, new dislocation half loops were nucleated from the surface while high-temperature dislocations still resisted motion (Fig. (c)).

Fig.11. X-ray topographs of a sample pulled in tension at 825°C under a stress of 380 gm/mm^2.

(a) specimen, before pulling, contains both straight (A) and curved (B) dislocations

(b) After pulling the sample see the straight dislocations moved under this load while the curved ones did not (From the curvature of the dislocation at B, one can calculate a residual stress of ~ 3Kgm/mm^2 acting on it).

Fig. 12. (a) A tensile specimen was cut from the crystal shown in Fig. 8 and was deformed in tension at 825°C under a stress of ~200 gm/mm^2 along $[1\bar{1}0]$. The screw dislocations($\bar{b} = \frac{a}{2}[\bar{1}01]$) get a shear stress of 88gm/mm^2. Observe that the dislocations did not move any appreciable distance (compare this topograph with Fig. 8).

(b) Topograph taken after heating the sample to 950°C for 15 minutes under a load of 20 gm/mm^2 along $[1\bar{1}0]$. The dislocations at B climbed towards the surface and intersected it.

(c) Deformation was continued at 900°C under a load of 380 gm/mm^2 along $[1\bar{1}0]$. Fresh dislocations were generated from the specimen edges, closer observation shows that the original high-temperature dislocations still did not appreciably.

Fig. 13. Generation and propagation of dislocations in an initially dislocation-free sample deformed in tension at 825°C. The same areas are shown after deforming for a) one-half hour, b and c) two hours, d) three dours and e) four and one-half hours. The applied load was 70 gm/mm in a) and 380 gm/mm in the remaining tests. Observe how dislocations are generated at the surface and travel into the sample as long loops. Though the general dislocation direction lies along $\langle 110 \rangle$ they are not strictly straight. The $(\bar{1}\bar{1}1)$ and $(1\bar{1}\bar{1})$ primary planes make steep angles to the surface of the sample and hence individual dislocations are not well resolved.

Fig. 14. Dislocation substructure in a sample deformed in tension at 950°C for 1/2 hour. Dislocations are generated from the surface in groups and travelled all across the width of the sample. A number of dislocation reactions have occurred to form two three-fold notes. The resultant dislocation with $b = \frac{a}{2}[1\bar{1}0]$ is out of

contrast (g.b=0).

Fig. 15. Topographs showing the dislocations generated in the sample by pulling under (a) 30 gm/mm^2 950°C for 30 minutes (b) 36 gm/mm^2 at 850°C for 30 minutes. (c) ~65gm/mm^2 at 900°C for 15 minutes. The veritical direction is along the tensile axis which makes 45° to [111] and [$\bar{1}$01] directions.

Fig. 16. Electron micrographs of thin foils of silicon made from highly deformed samples.

a) Bundles of edge-dislocations on the main slip plane. A narrow dipole attached to the main dislocation is denoted by (A), isolated dipoles by (B) and small dots by (C).

b) Long dipoles and large loops are shown by (A) and (B) respectively. See how a straight dislocation abruptly changes its direction by 90° at (C). Also note four-fold dipole-confluences.

c) Another area showing that dislocations are not perfectly straight.

d) A large link-loop on a moving screw dislocation.

e) An area showing long dipoles and loops. A large cusp is formed on the dislocation at (A).

f) A large loop changing its orientation rather abruptly.

g) Bundles of edge dislocations and a possible example of dislocation interaction at (A).

Fig. 17. The position of dislocations before (a) and after (b) the tensile test at 825°C, under a resolved shear stress of 36 gm/mm^2. In (a) the isolated dislocations are labelled and their velocities are listed in Table II.

Fig. 18. Dislocations before (a) and after (b) the tensile test at 850°C under resolved shear stress of 36 gm/mm^2. Topograph (c) and (d) show the continuation of the test at 800°C and 775°C respectively.

Fig. 19. Dislocations before (a) and after (b) the tensile test at 900°C under a tensile load of 36gm/mm^2. Topograph (c) shows the positions of the dislocations after continuing the test at 920°C.

Fig. 20. A plot of dislocation velocities against the reciprocal of temperature for nearly screw dislocationsunder a resolved shear stress of 36 gm/mm^2. The upper line is for nearly straight dislocations, while the lower line is for curved dislocations.

Fig. 21. A plot of dislocation velocities against the reciprocal of temperature for nearly 60°- segments.

Fig. 22. The motion of a screw dislocations with jogs of varying sizes (see test for illustration).

Fig. 23. a) The dislocation AB of nearly screw orientation bows out between the pinning points. The dots represent vacancies in voids in the lattice.

b) The dislocation after bowing out is in exact screw orientation at the middle while towards it's either side is in nearby screw orientation with a small edge component.

c) The dislocation acquires a large jog due to climb.

d) Cross-over of the loop by climb and glide (see text for explanation.

Fig. 24. A plot of lograithm of distances between jogs against the reciprocal of temperature.

Fig. 25. A screw dislocation bowing-out between thermal jogs spaced at a distance l_j along the line.

Fig. 26. The bow out of a dislocation between jogs due to Peierls'-Nabarro force (see text for illustration).

Fig. 27. A plot of ($\ell n\ v + 1/2\ \ \ell n\ kT$) against $\frac{1}{T}$ for screw dislocations as derived from Fig. 25.

Fig. 28. Annihilation of kink-pairs on a dislocation line at a distance ℓ_m.

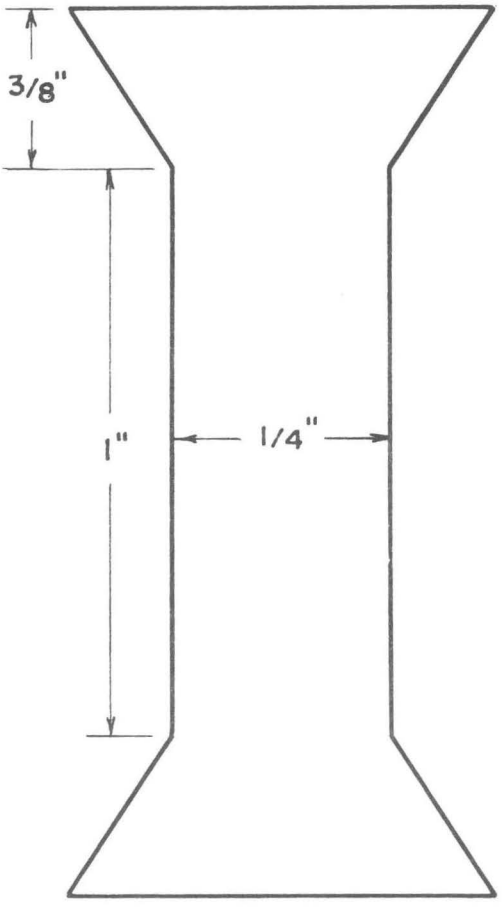

XBL 691-6

Fig. 1

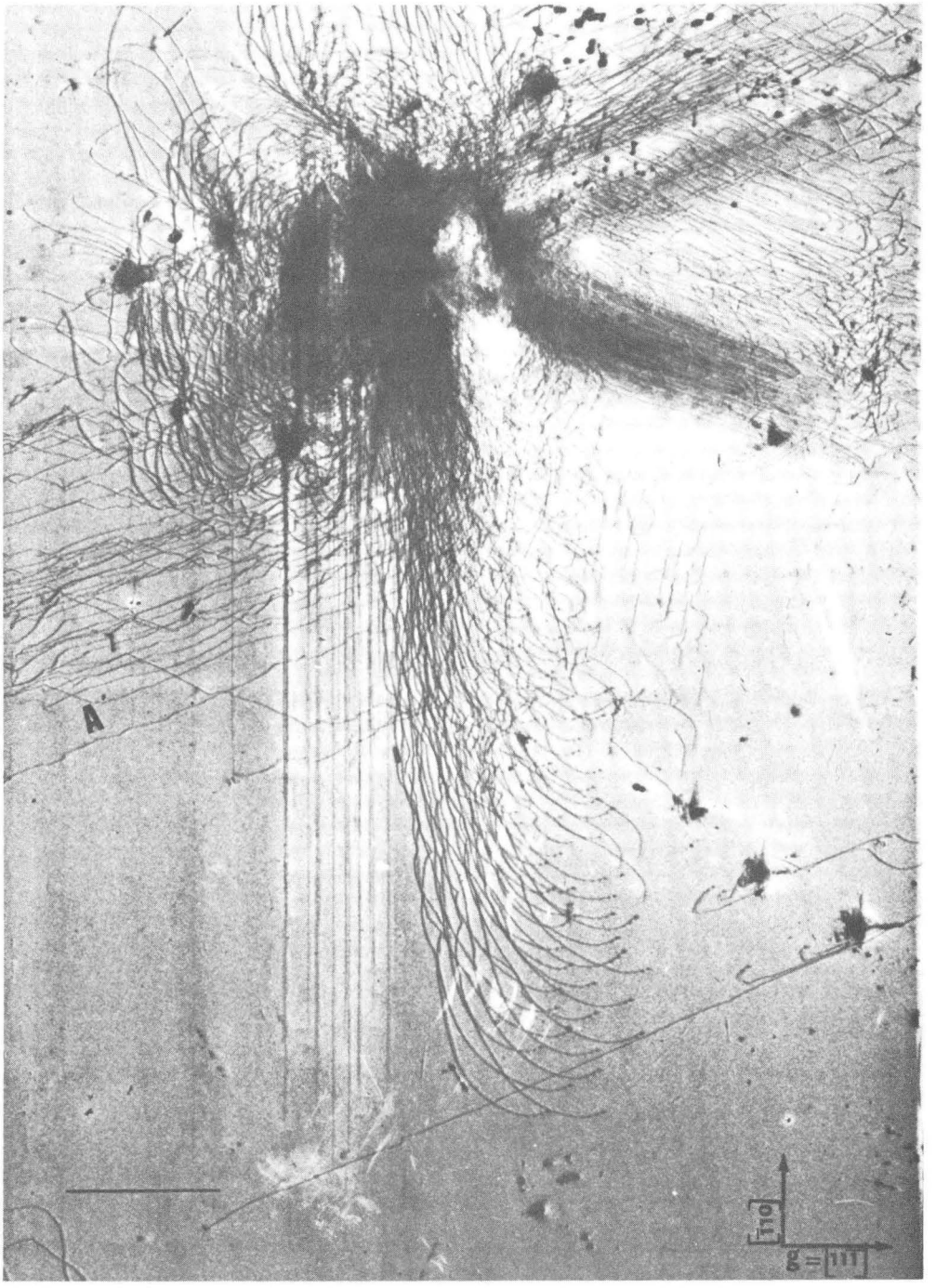

XBB 6812-7433

Fig. 2

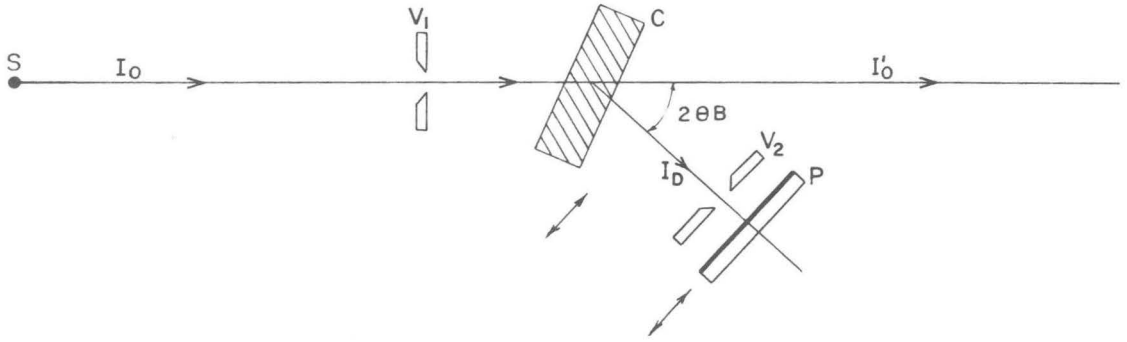

XBL 691-8

Fig. 3

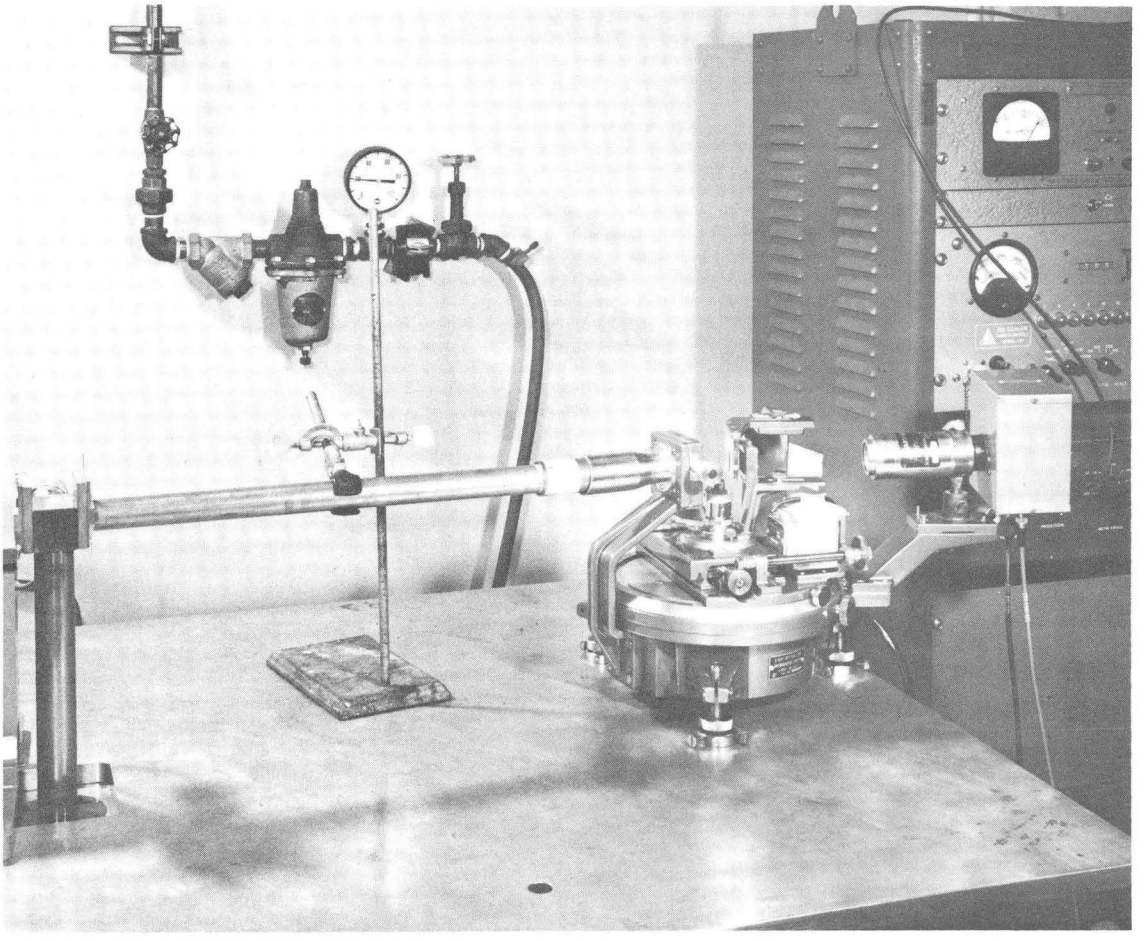

XBB 678-4978

Fig. 4

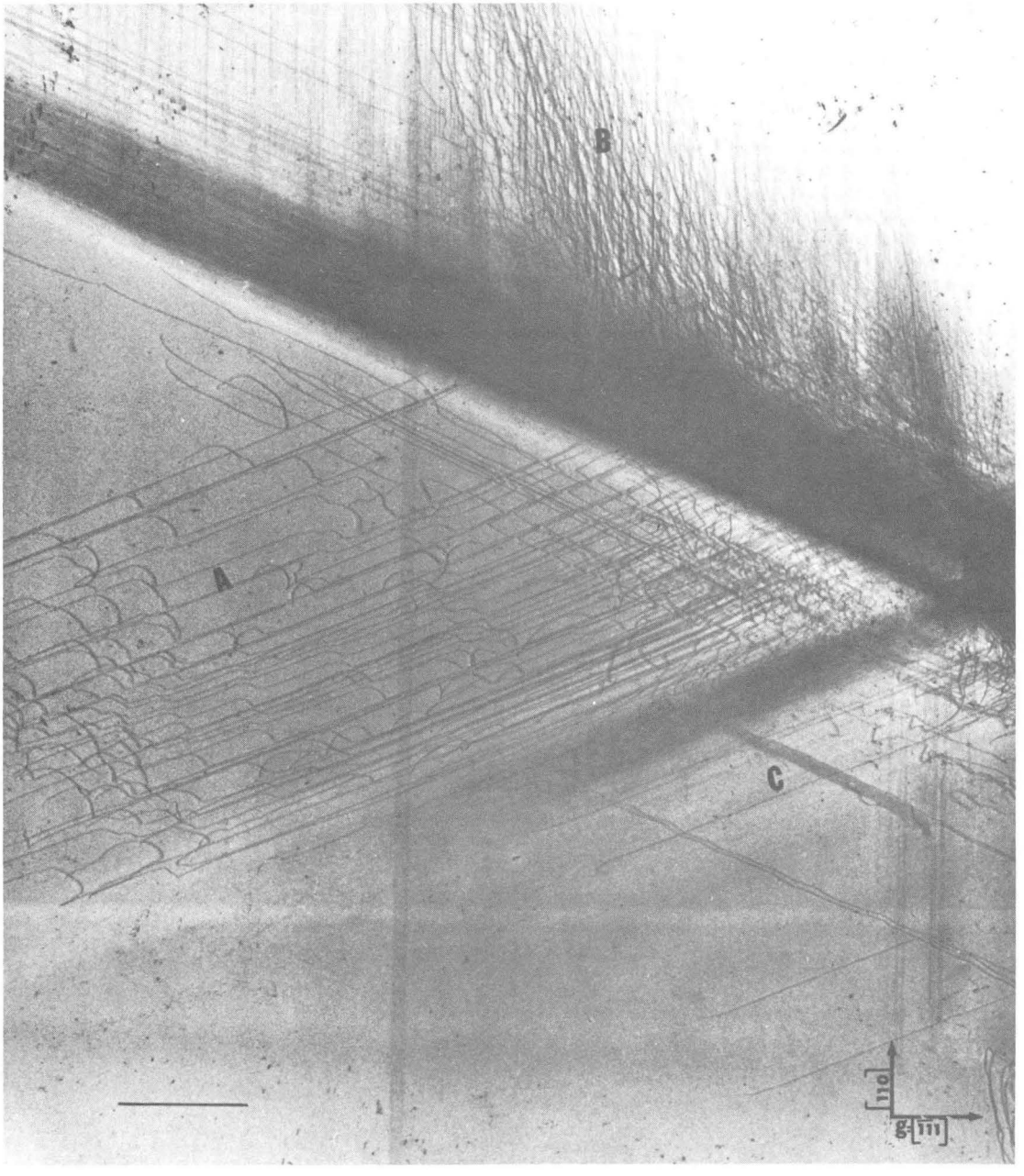

XBB 6812-7423

Fig. 5a

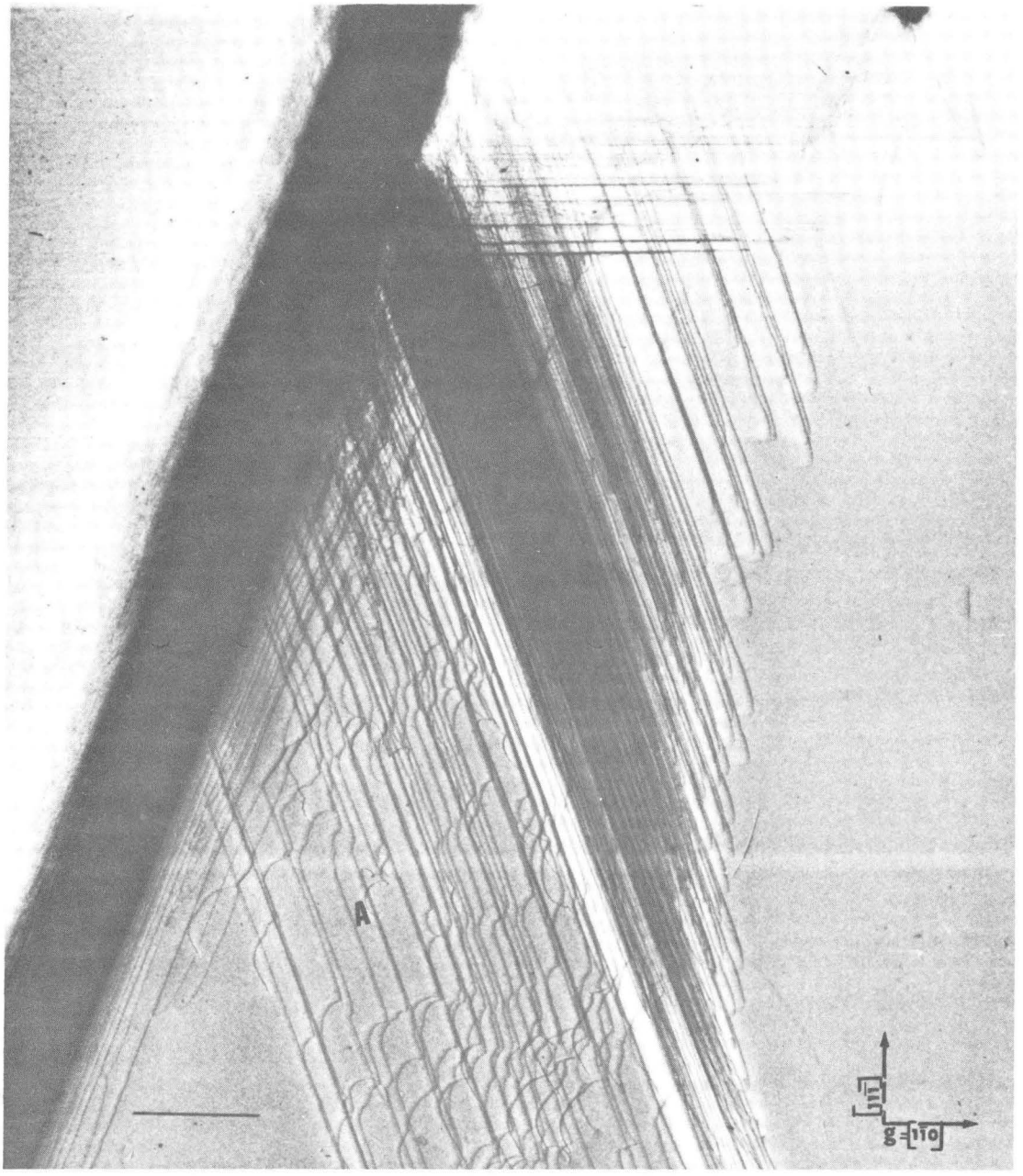

XBB 6812-7422

Fig. 5b

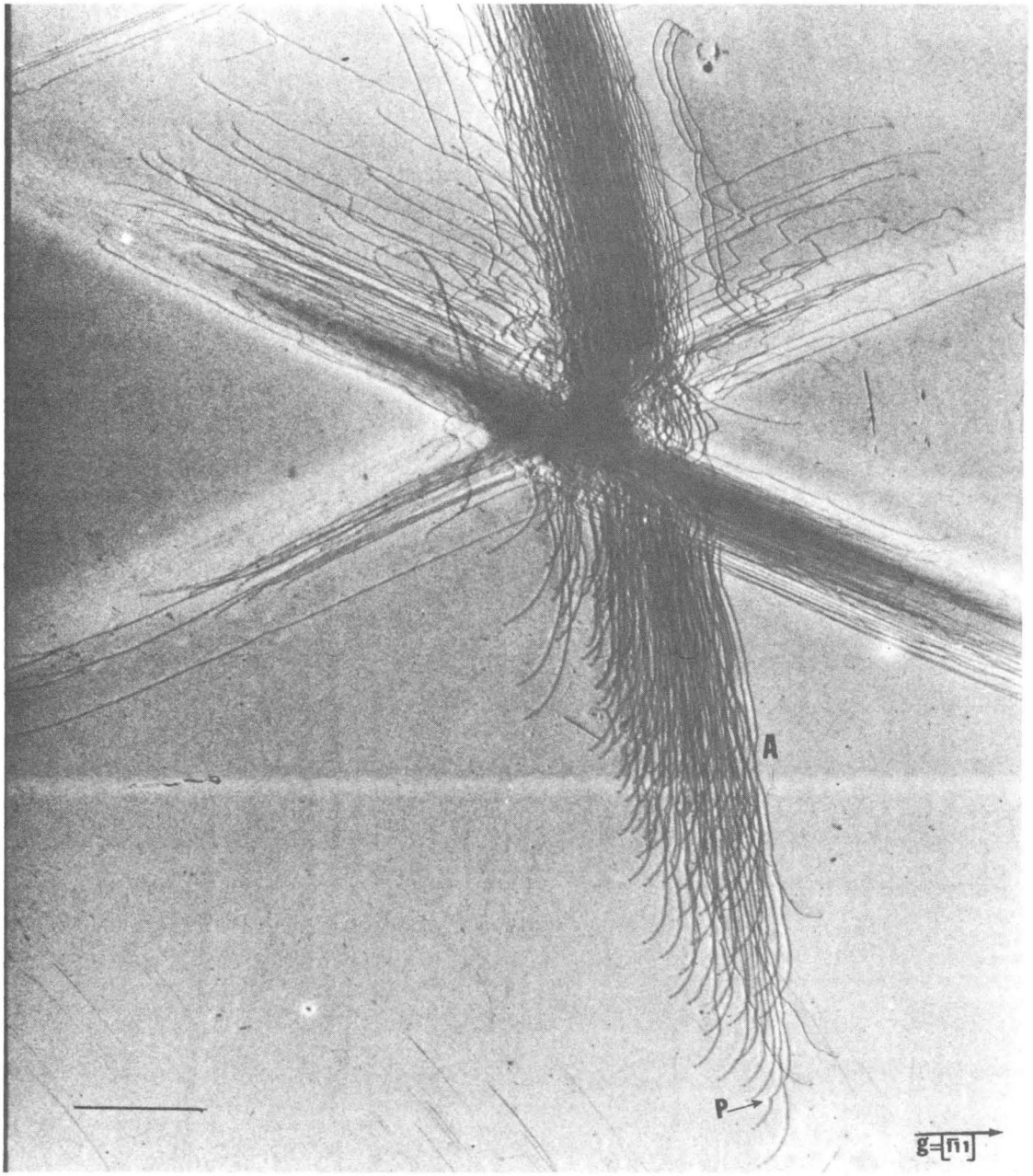

XBB 6812-7421

Fig. 6a

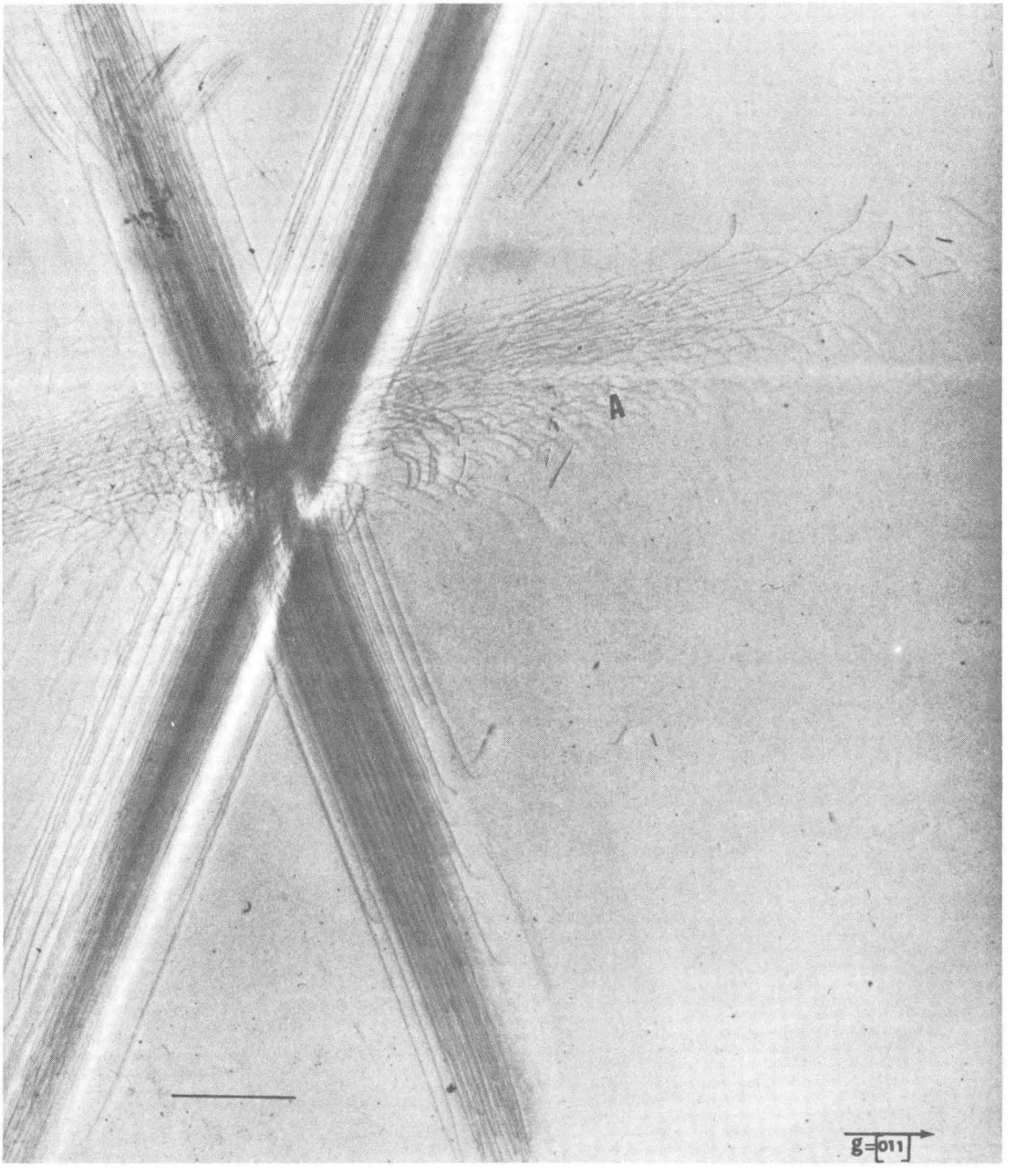

XBB 6812-7436

Fig. 6b

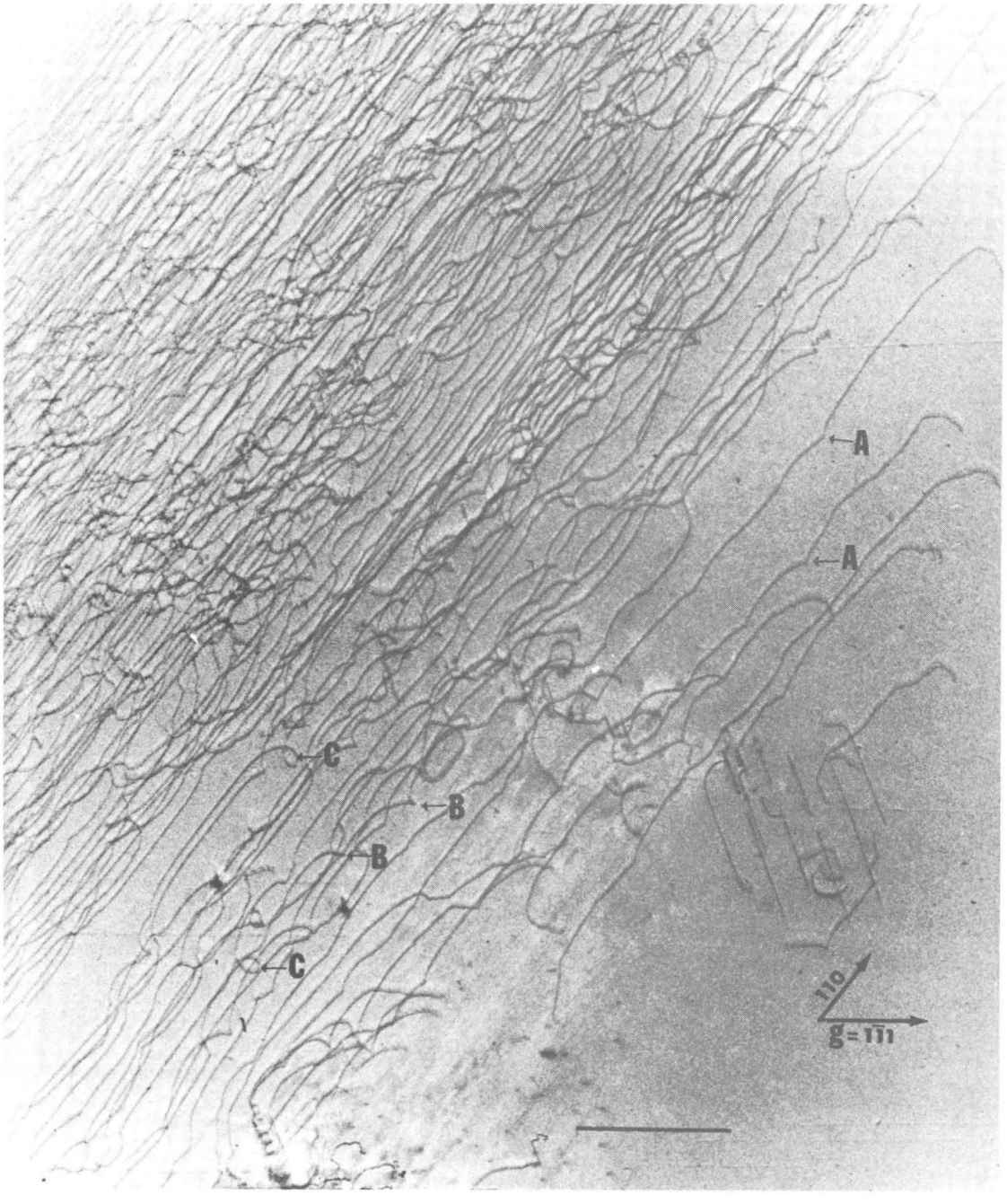

XBB 6812-7432

Fig. 7

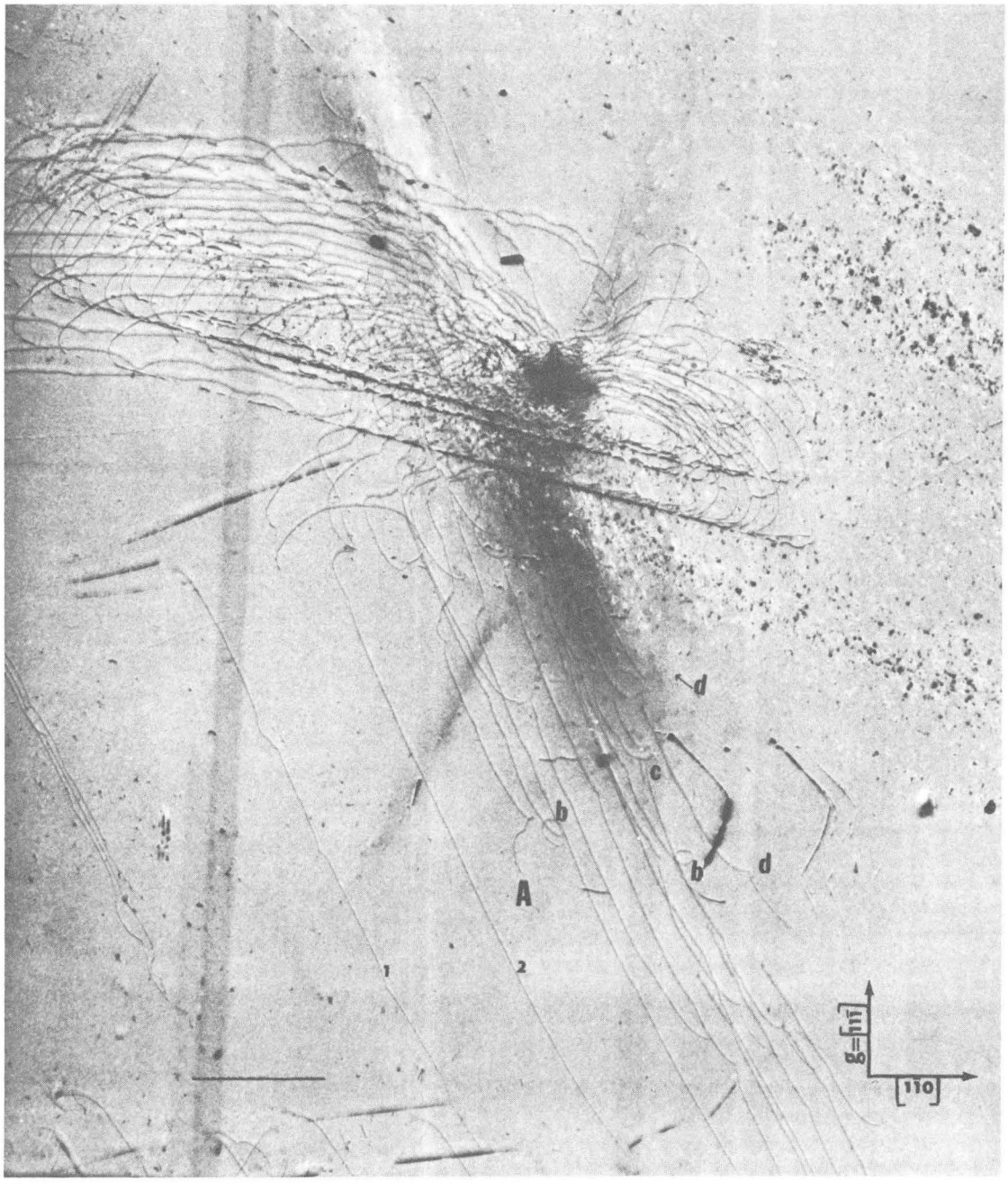

XBB 6812-7430

Fig. 8

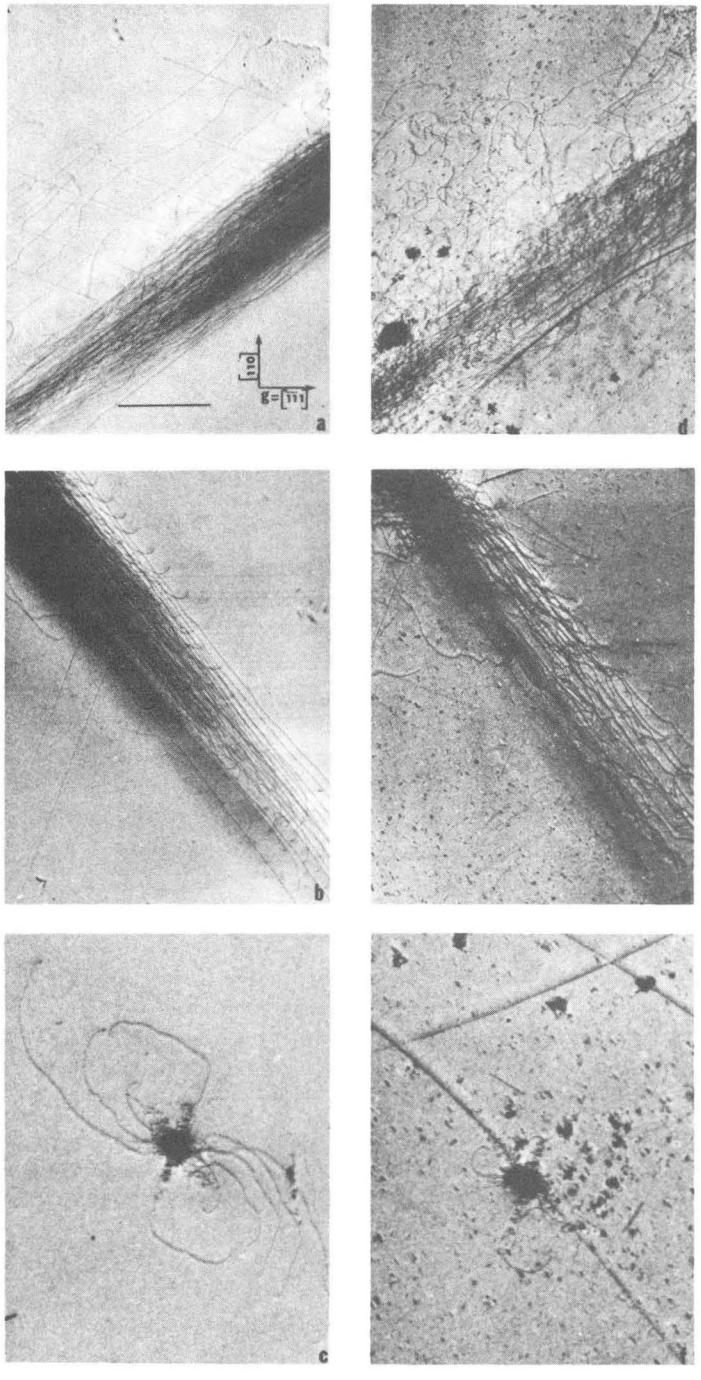

XBB 6812-7437

Fig. 9

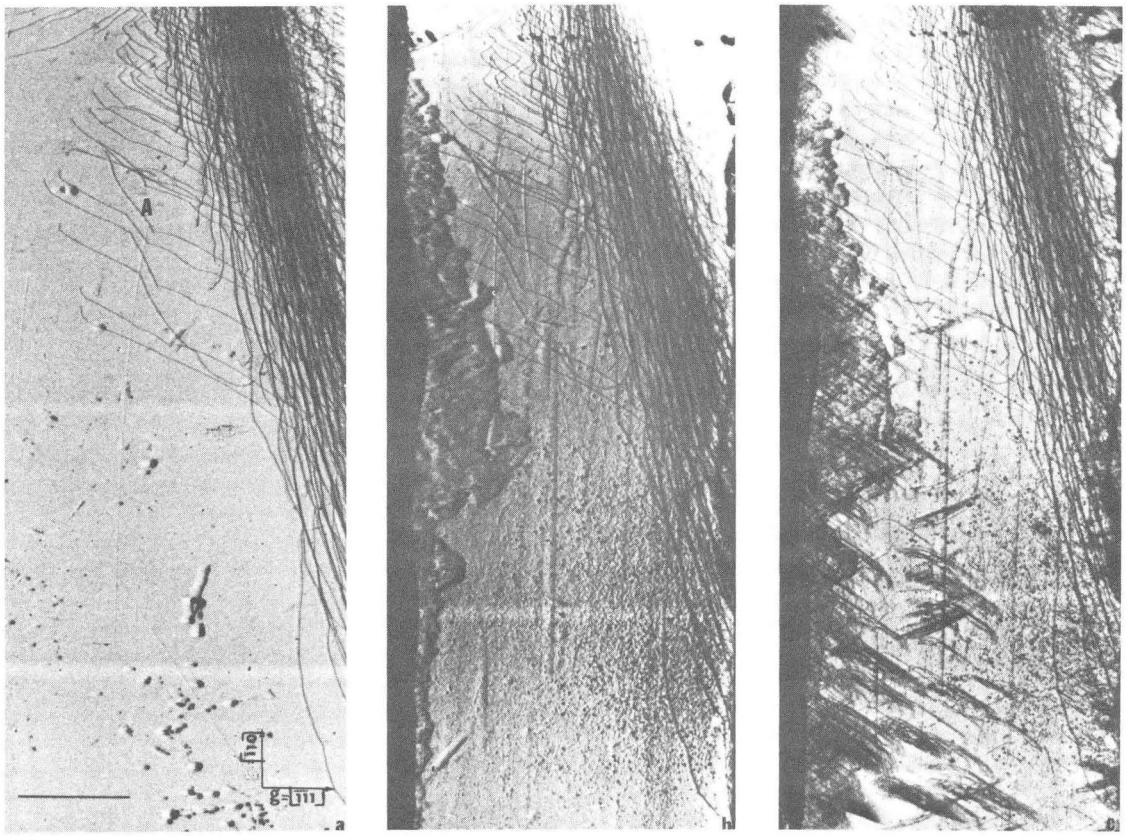

XBB 6812-7426

Fig. 10

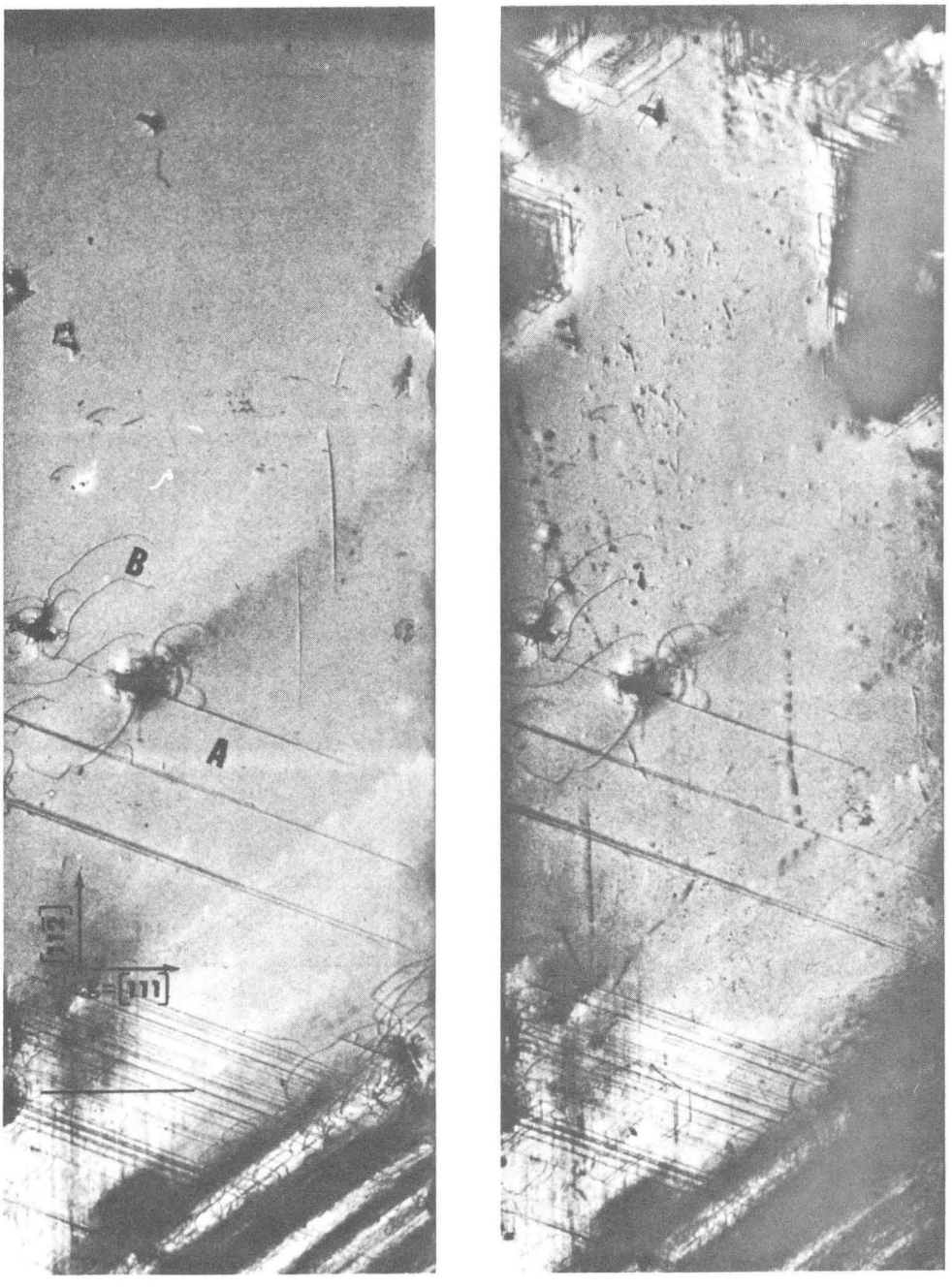

a b

XBB 6812-7447

Fig. 11

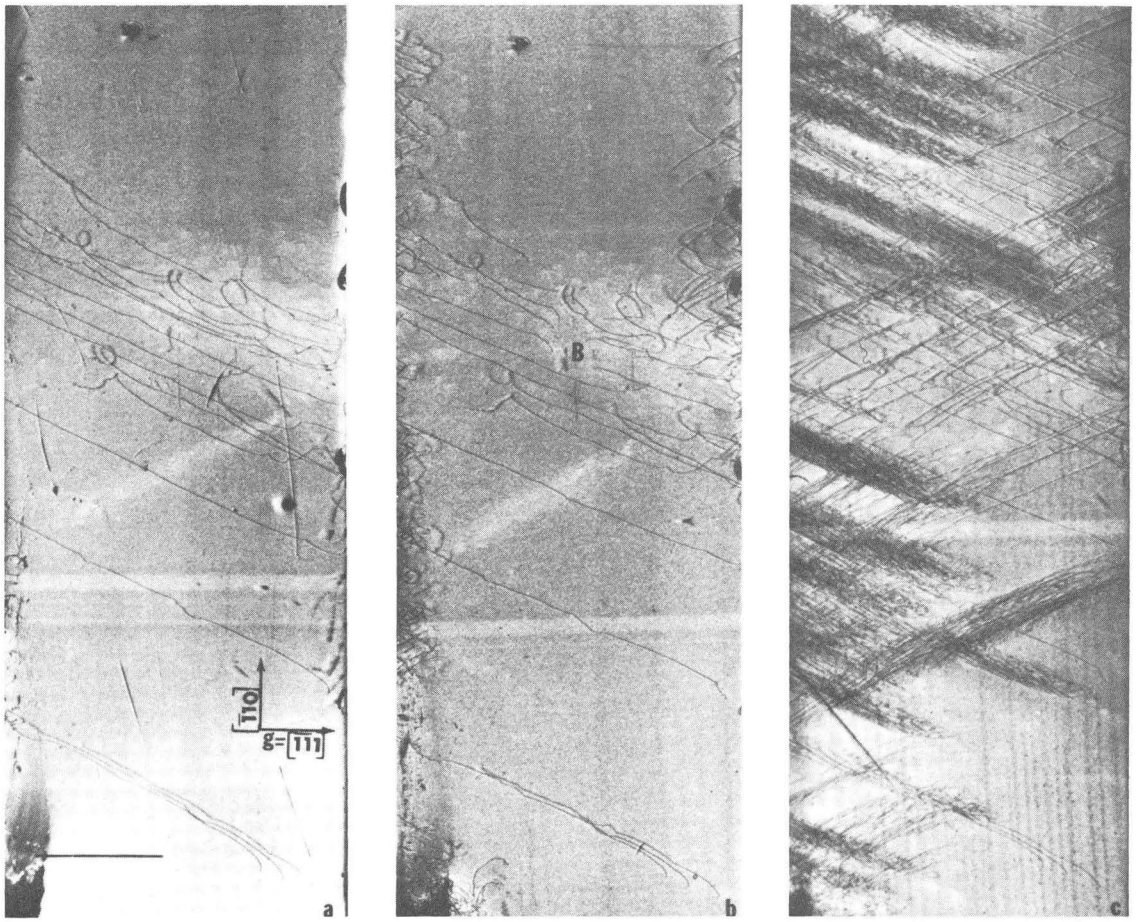

XBB 6812-7424

Fig. 12

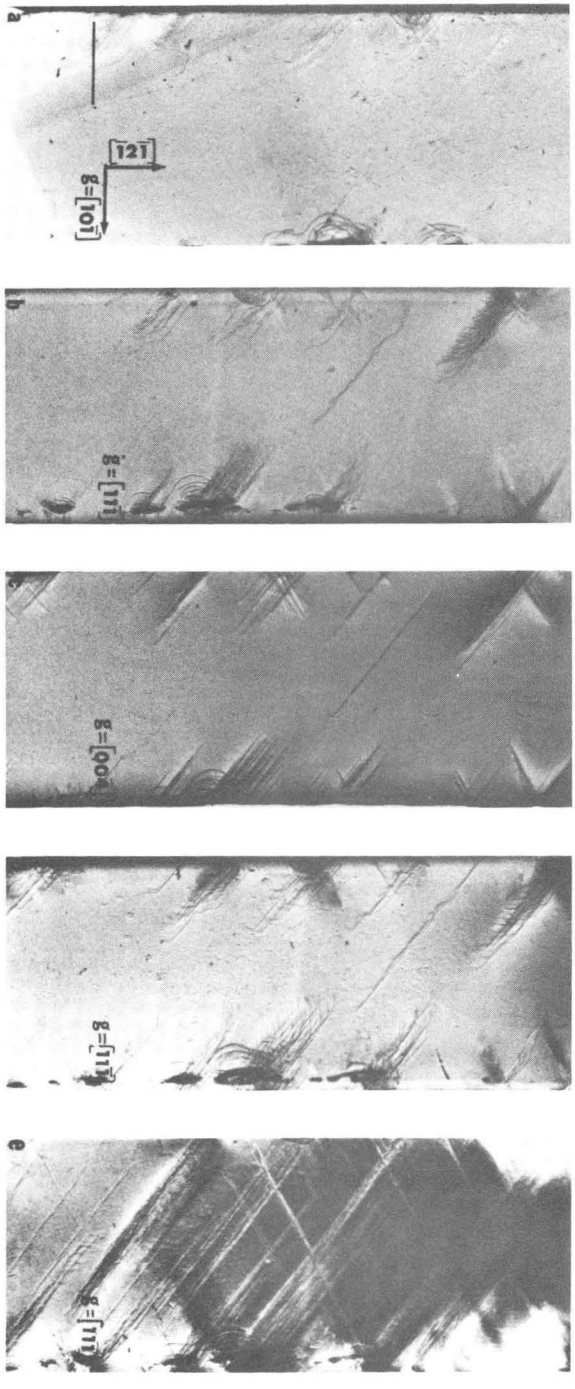

XBB 6812-7435

Fig. 13

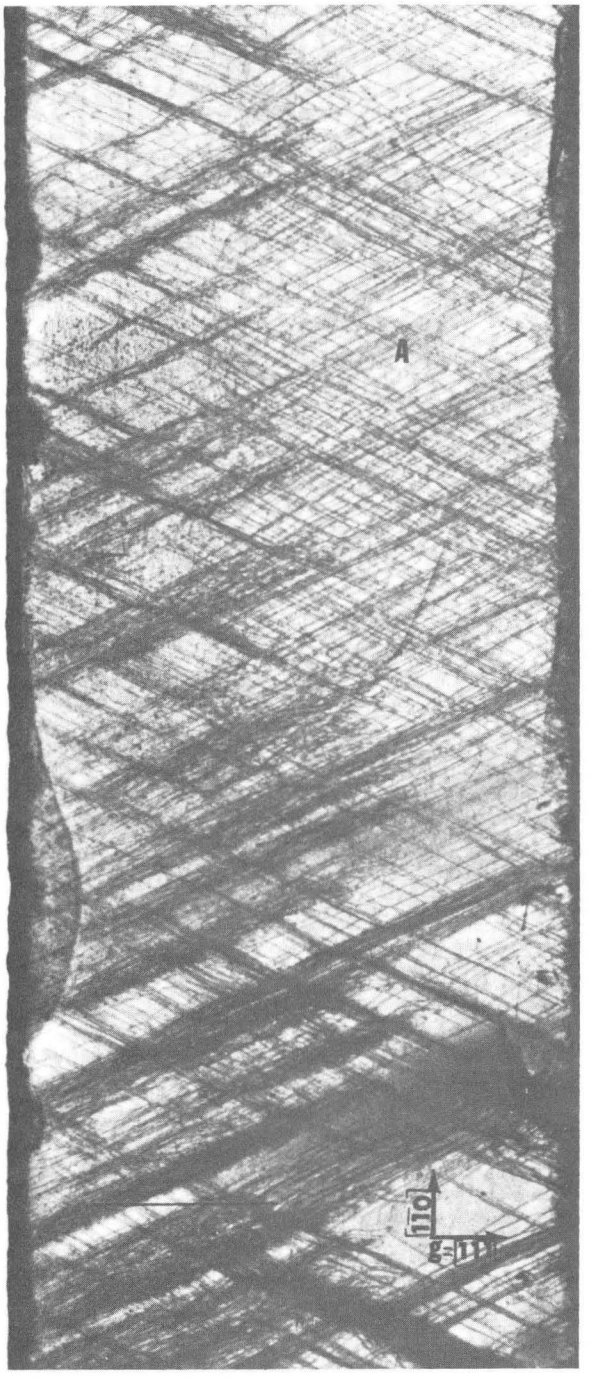

XBB 6812-7446

Fig. 14

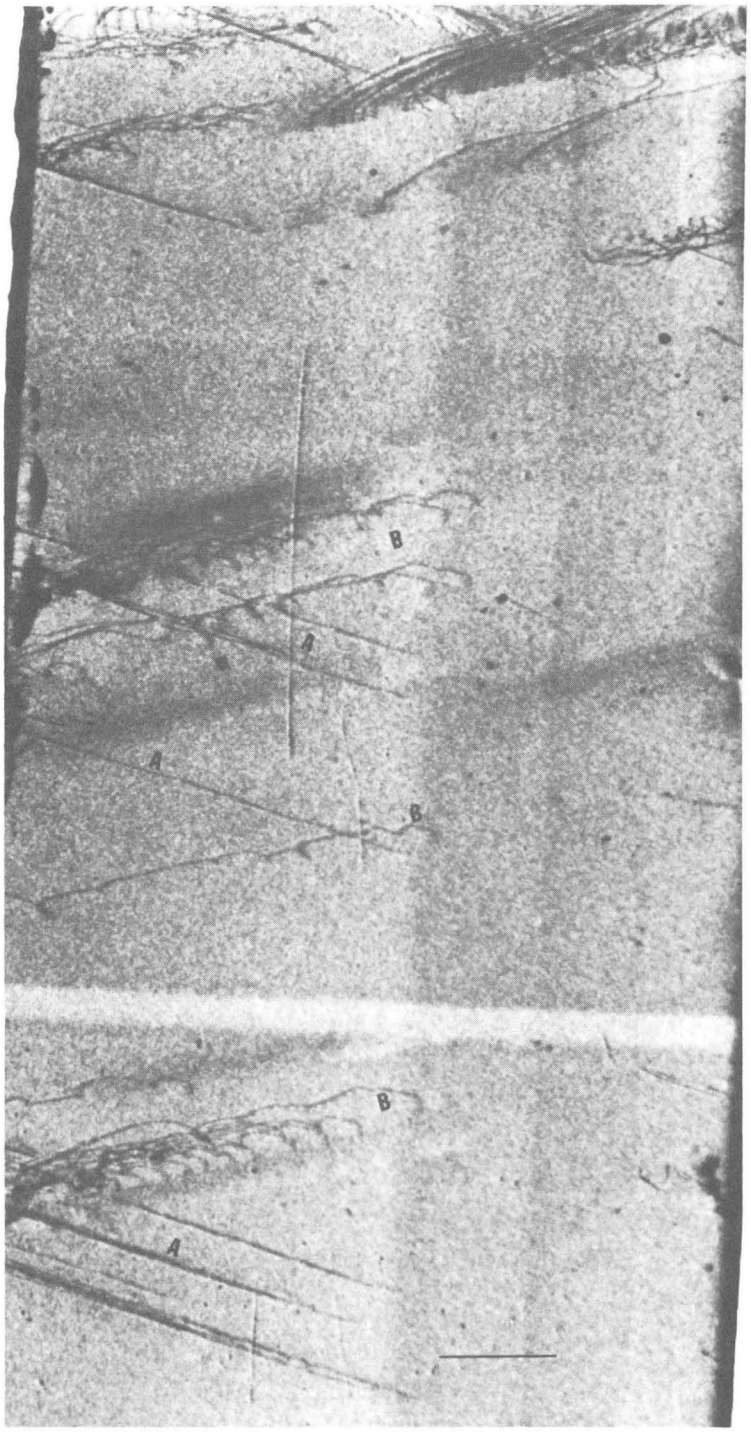

XBB 6812-7420

Fig. 15a

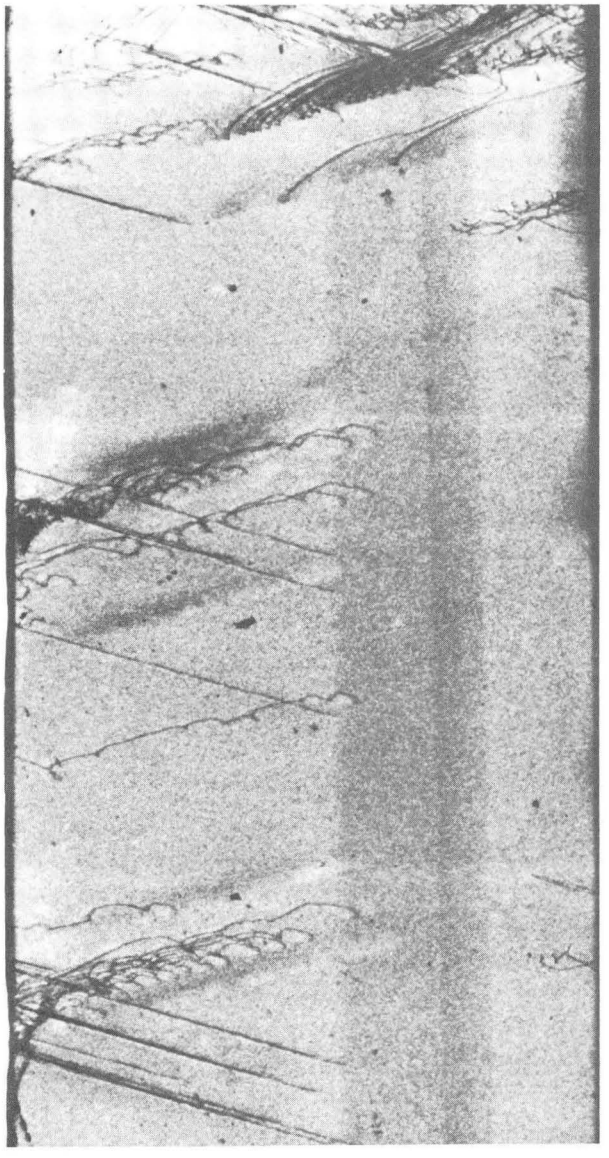

XBB 6812-7443

Fig. 15b

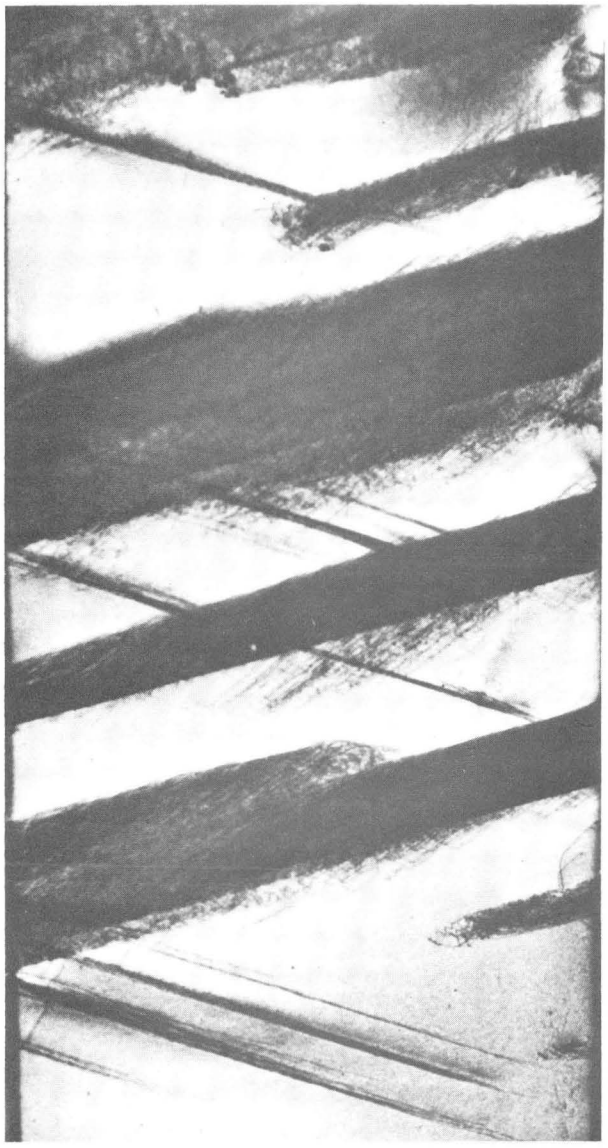

XBB 6812-7444

Fig. 15c

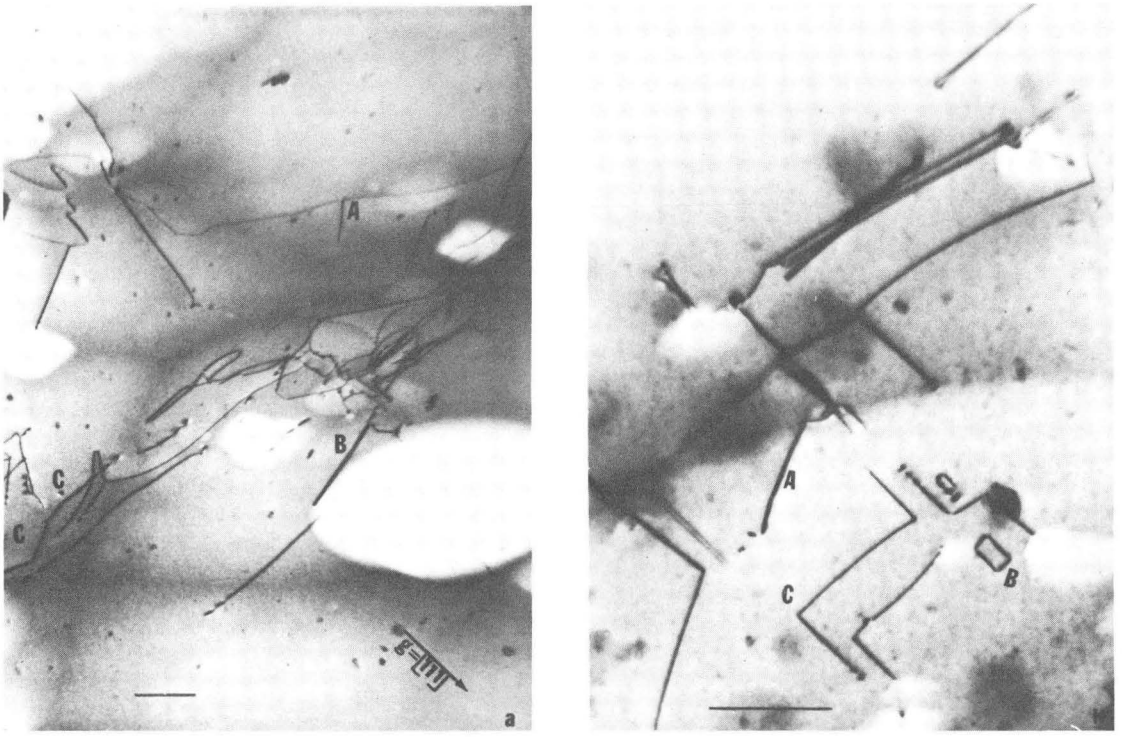

XBB 6812-7429

Fig. 16a & b

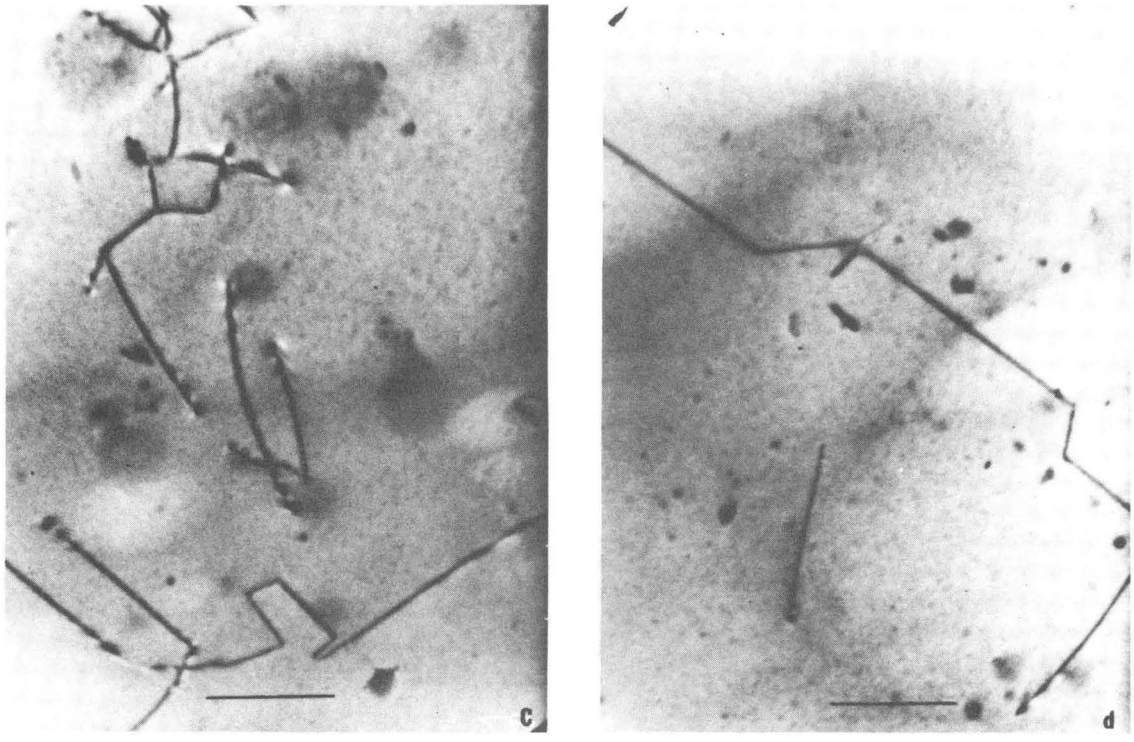

XBB 6812-7427

Fig. 16c & d

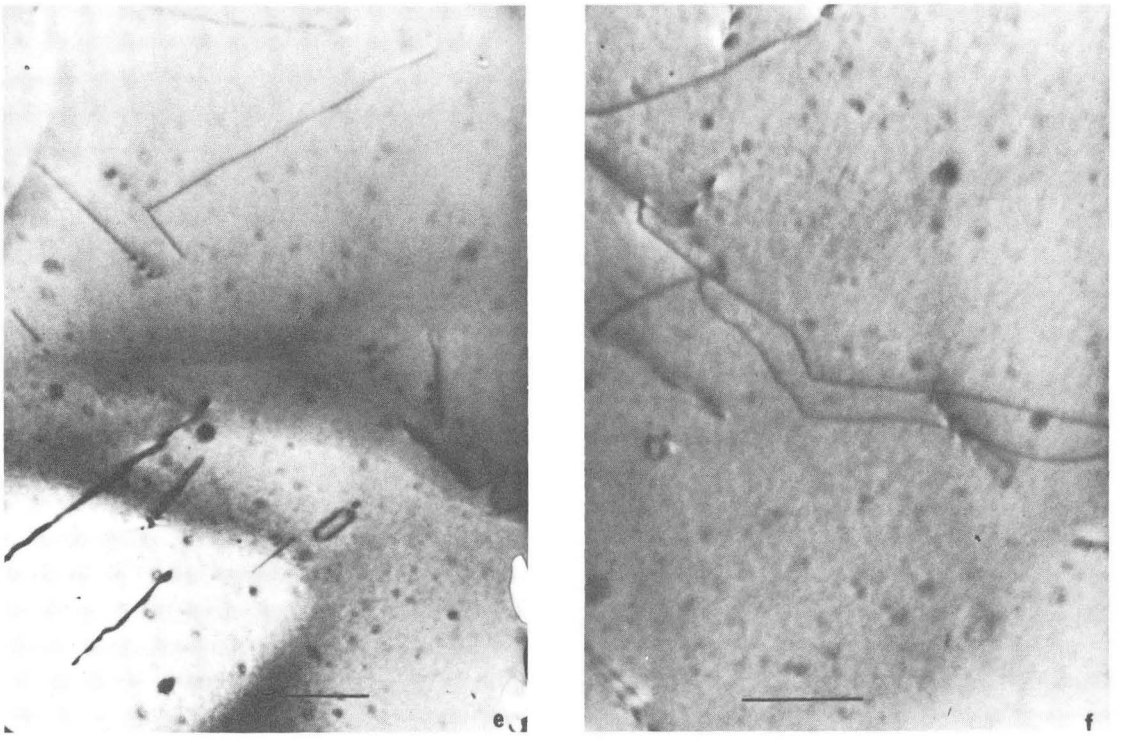

XBB 6812-7428

Fig. 16e & f

XBB 6812-7431

Fig. 16 g

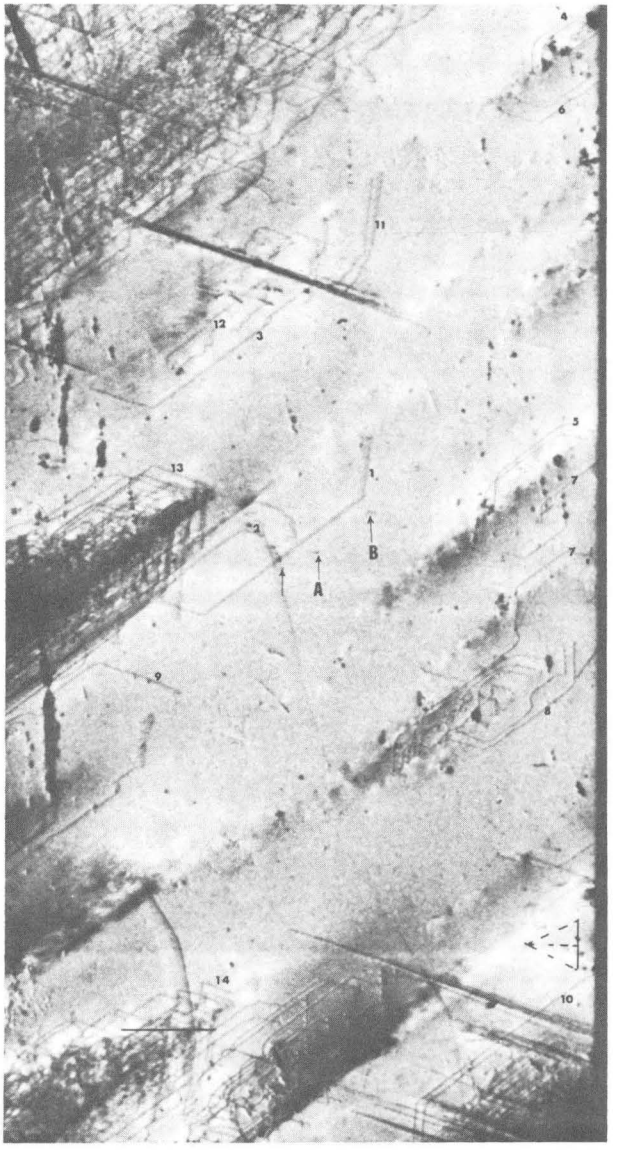

XBB 6812-7442

Fig. 17a

XBB 6812-7434

Fig. 17b

XBB 6812-7440

Fig. 17c

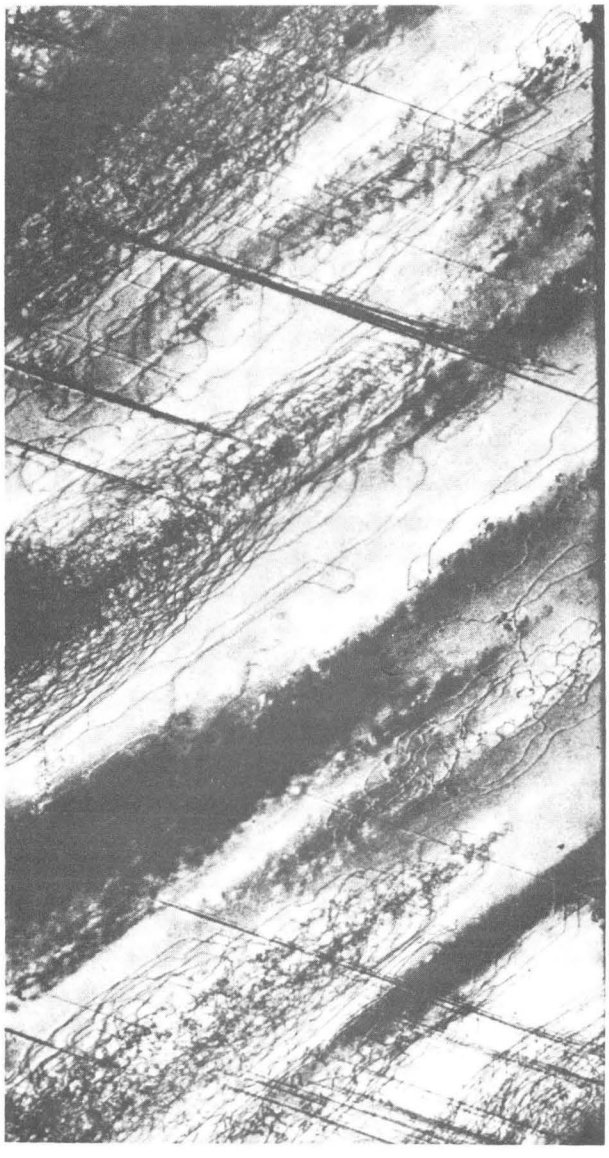

XBB 6812-7441

Fig. 17d

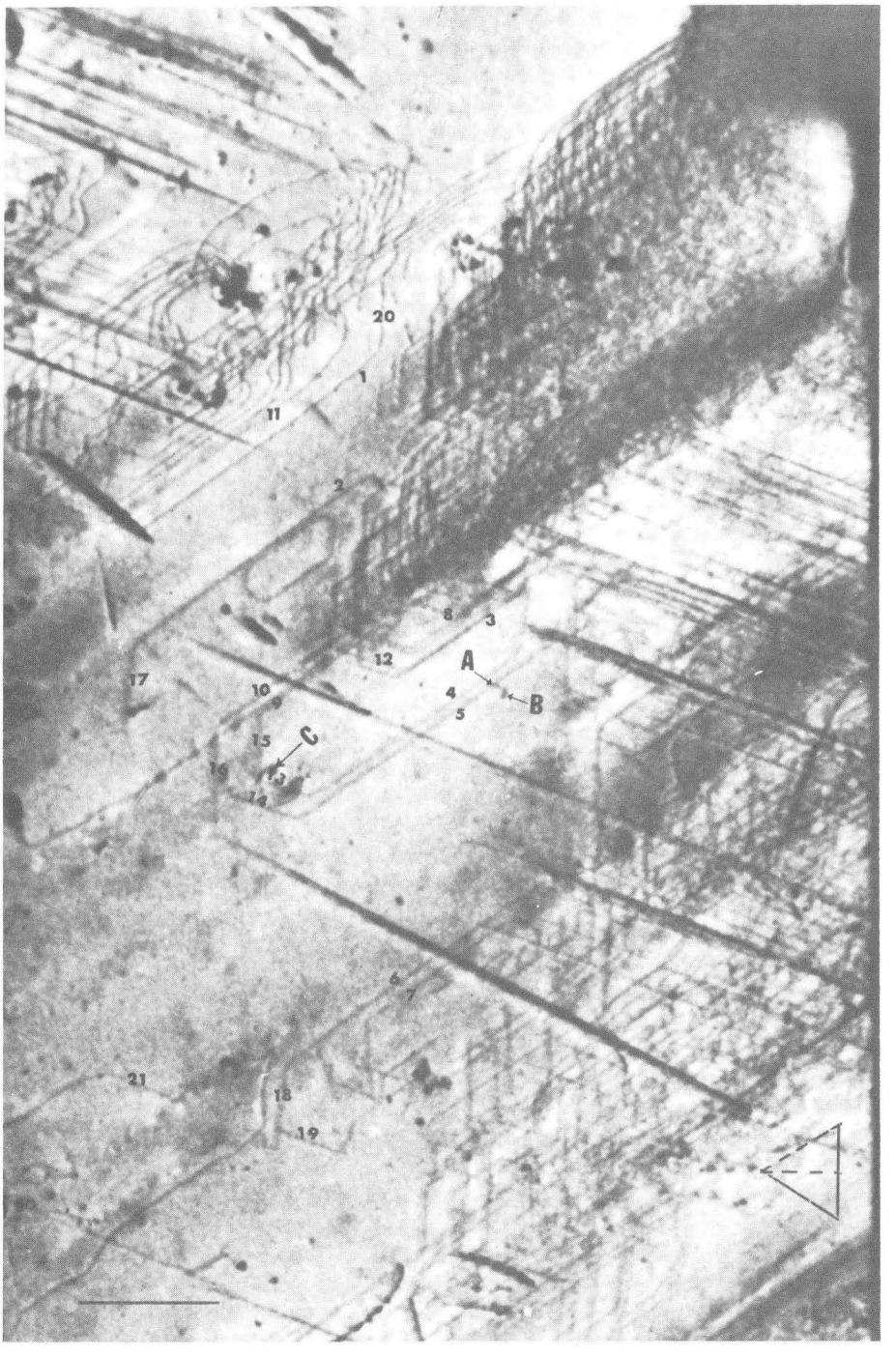

XBB 6812-7419

Fig. 18a

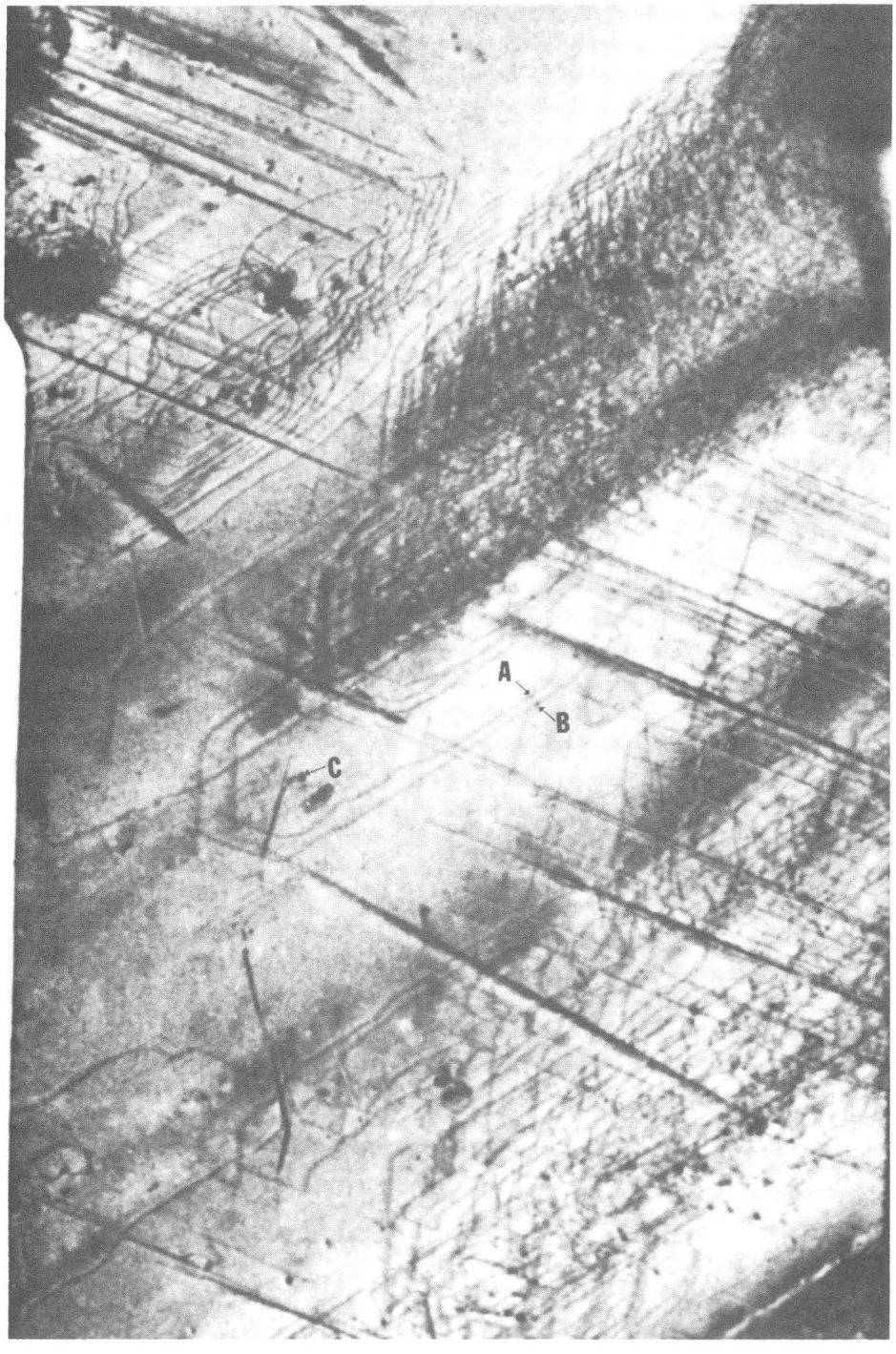

XBB 6812-7425

Fig. 18b

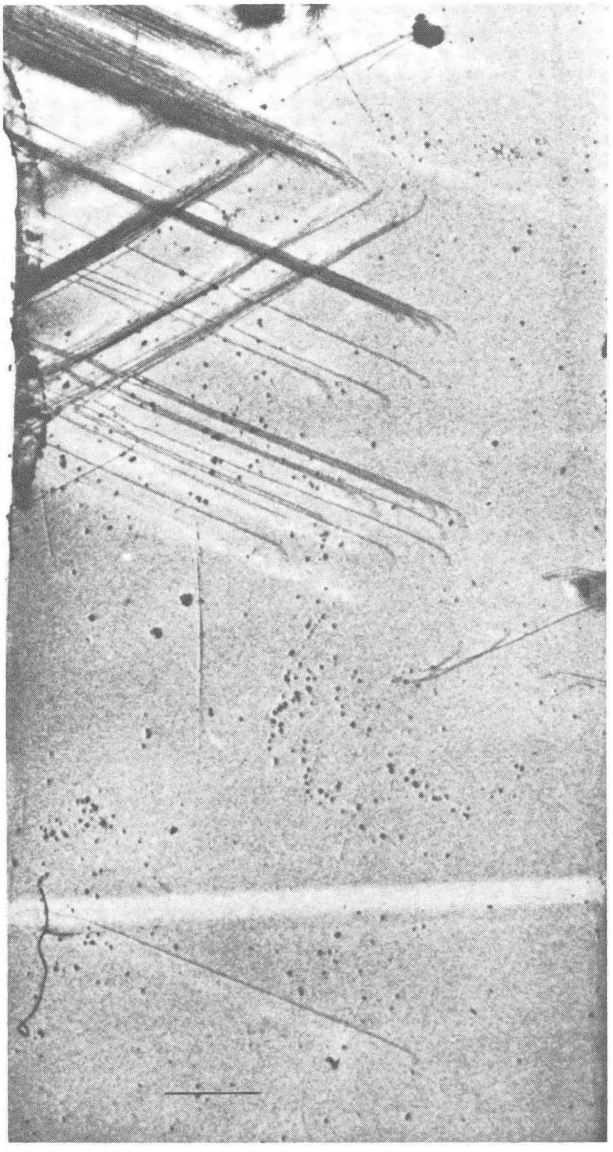

XBB 6812-7438

Fig. 19a

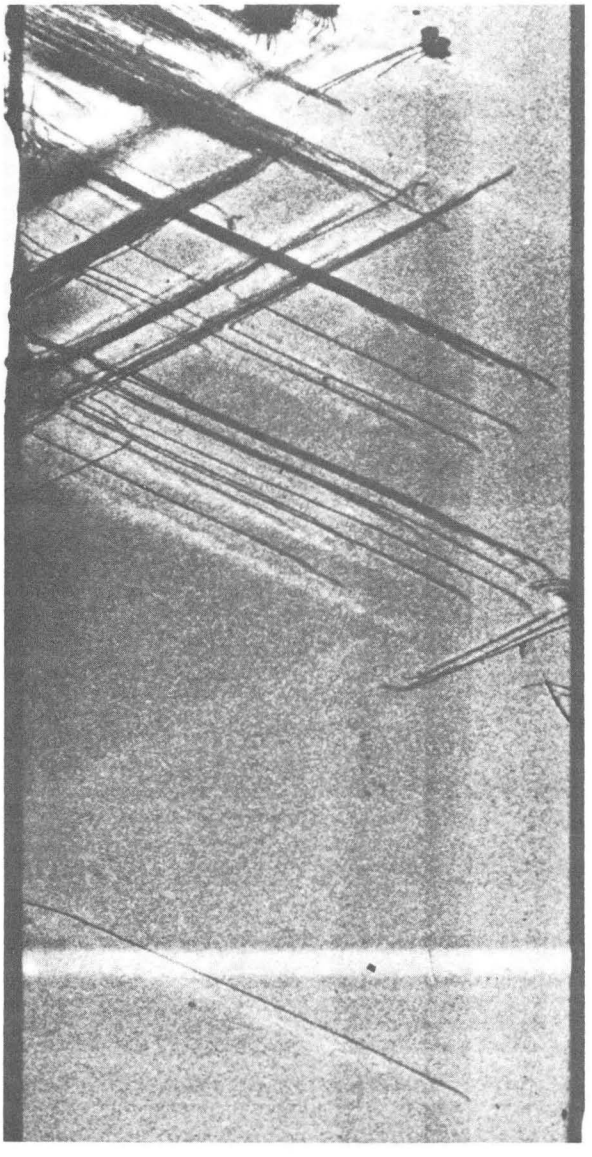

XBB 6812-7439

Fig. 19b

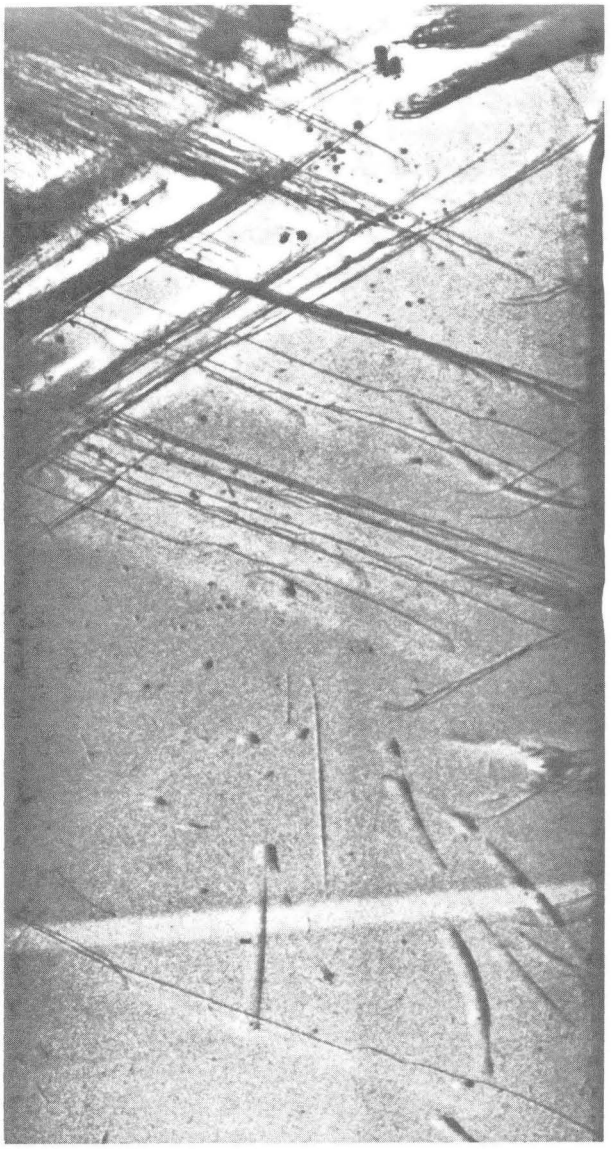

XBB 6812-7445

Fig. 19c

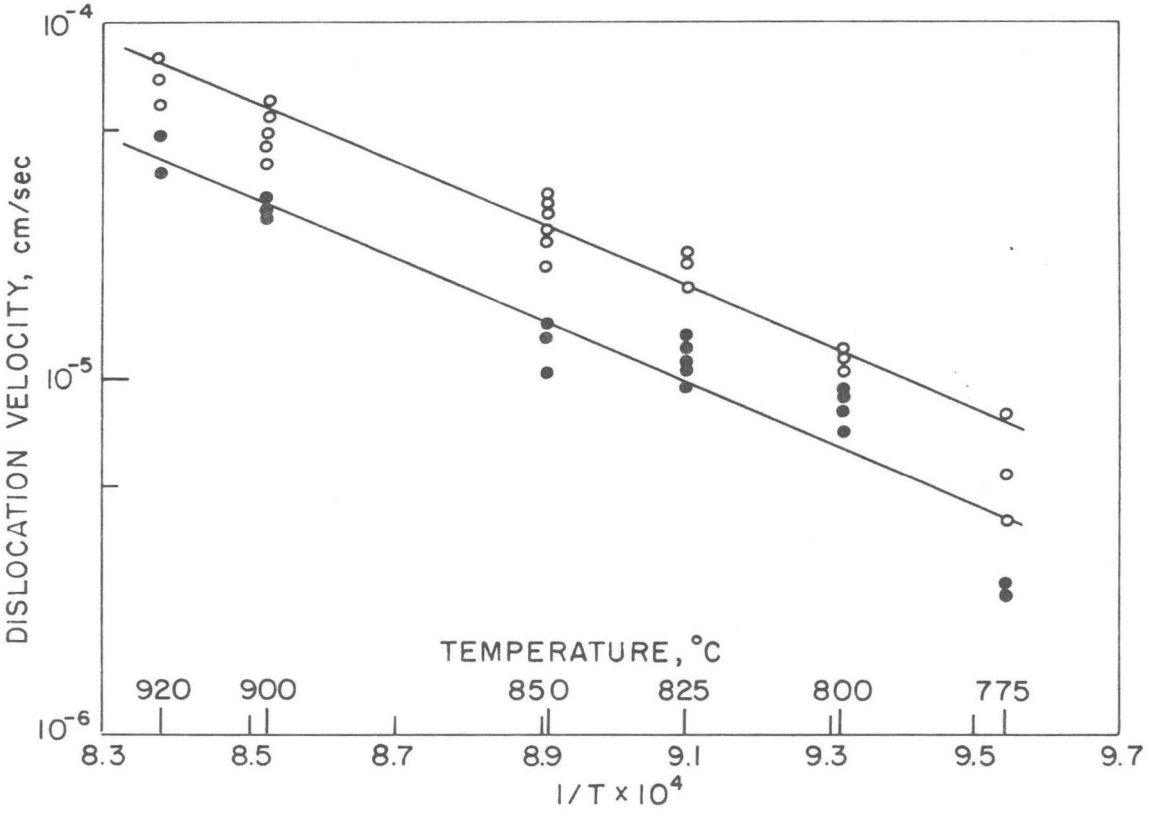

XBL 691-3

Fig. 20

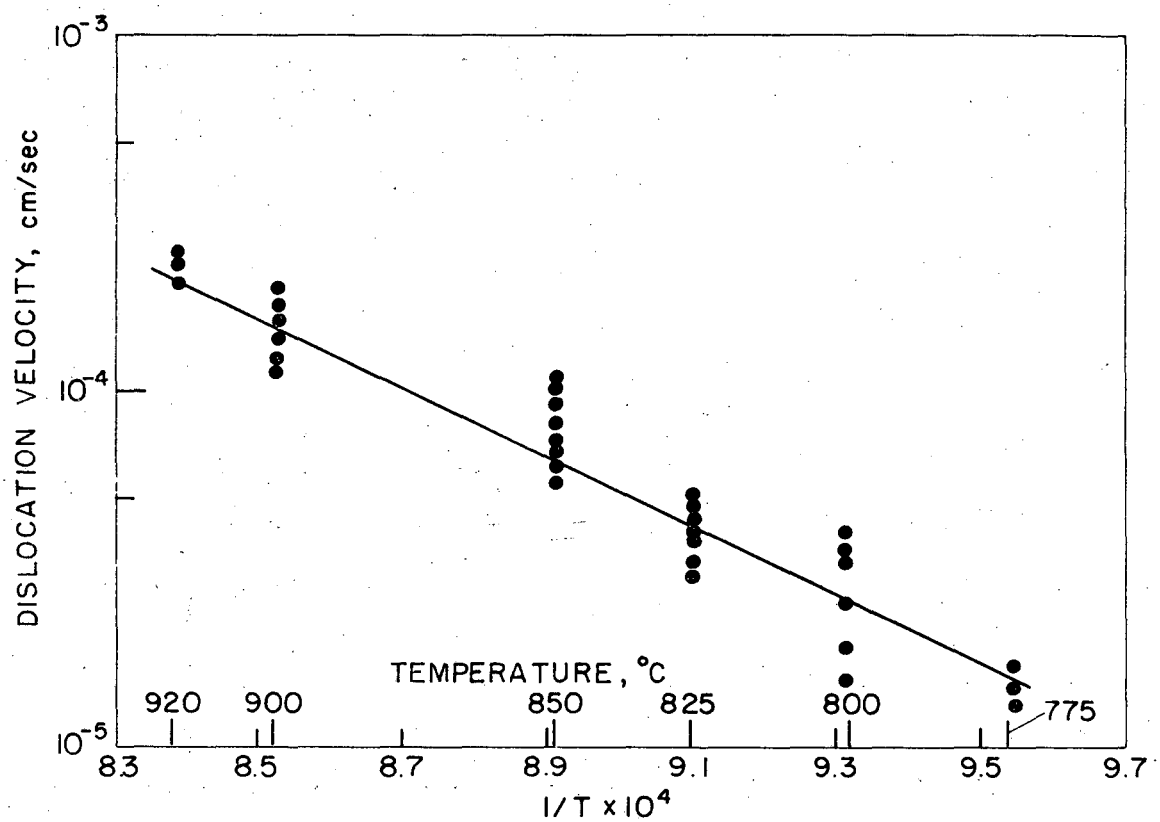

XBL 691-2

Fig. 21

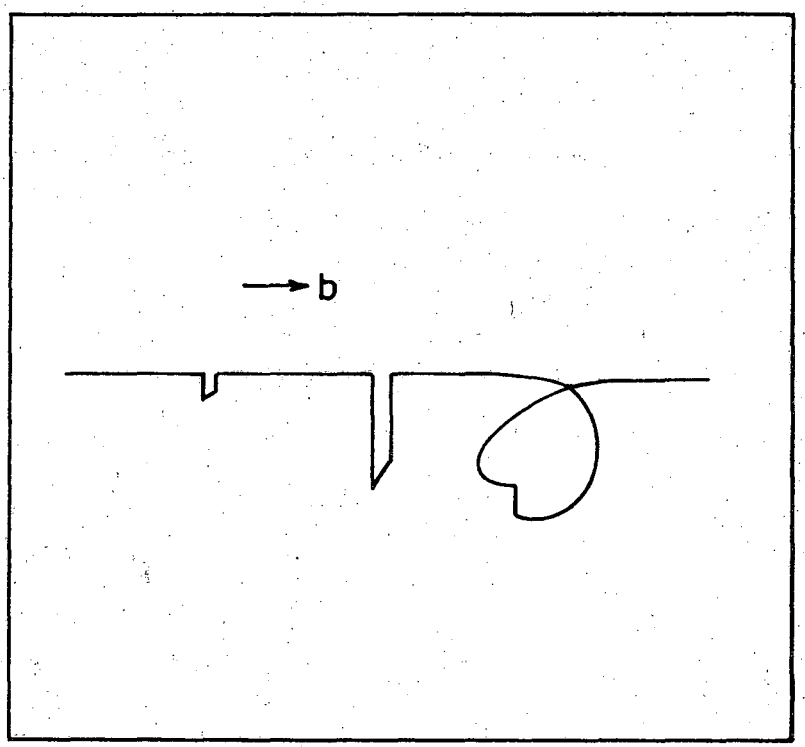

XBL 691-9

Fig. 22

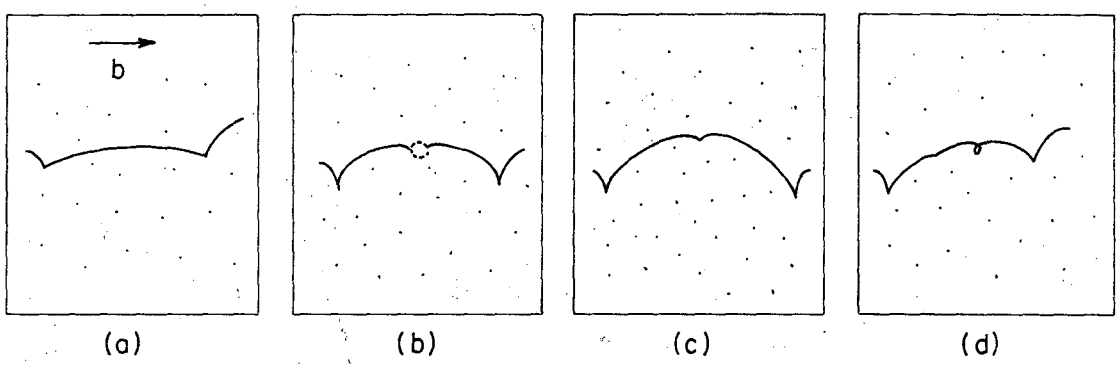

XBL 691-10

Fig. 23

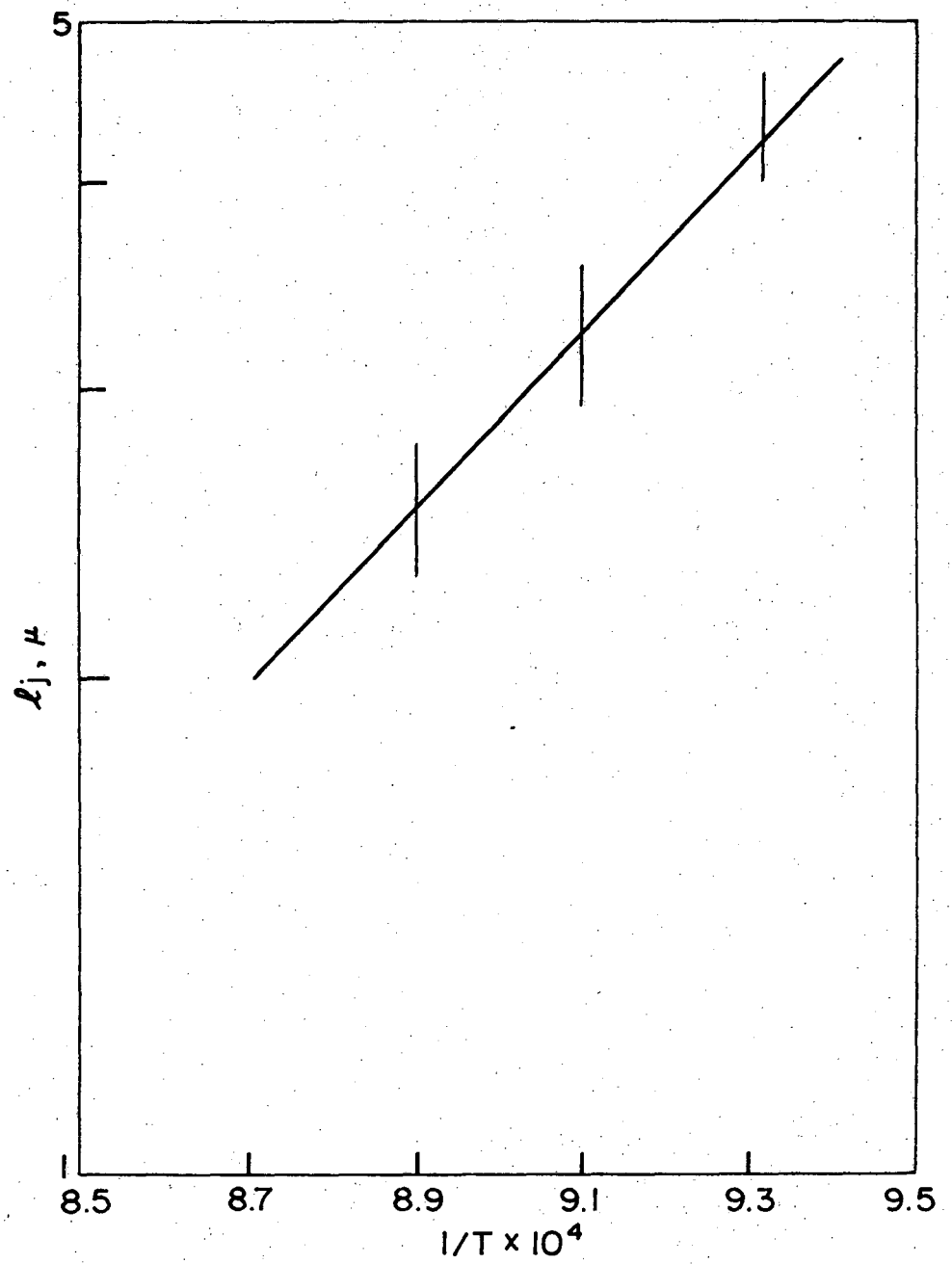

XBL 691-5

Fig. 24

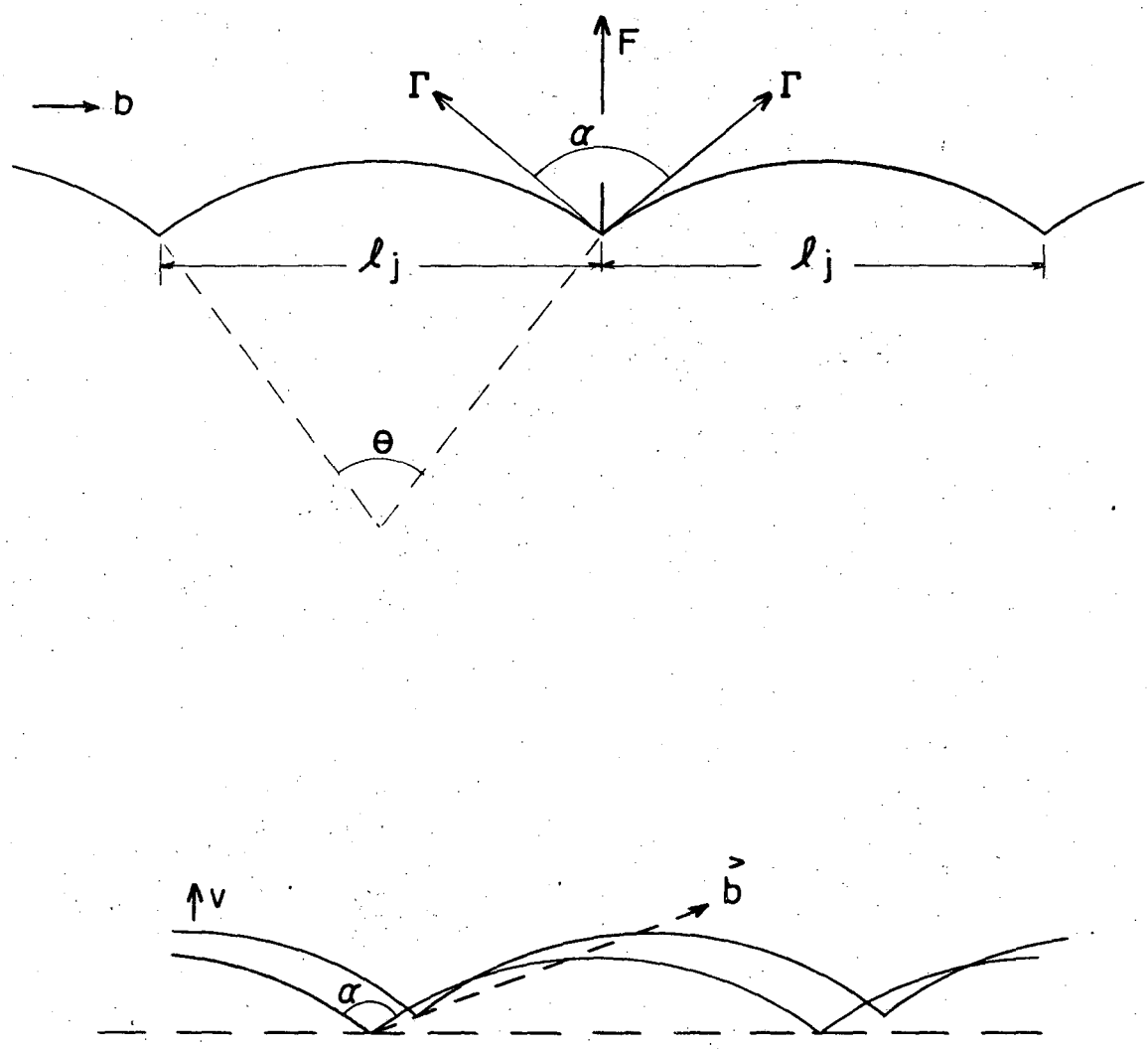

XBL 691-4

Fig. 26

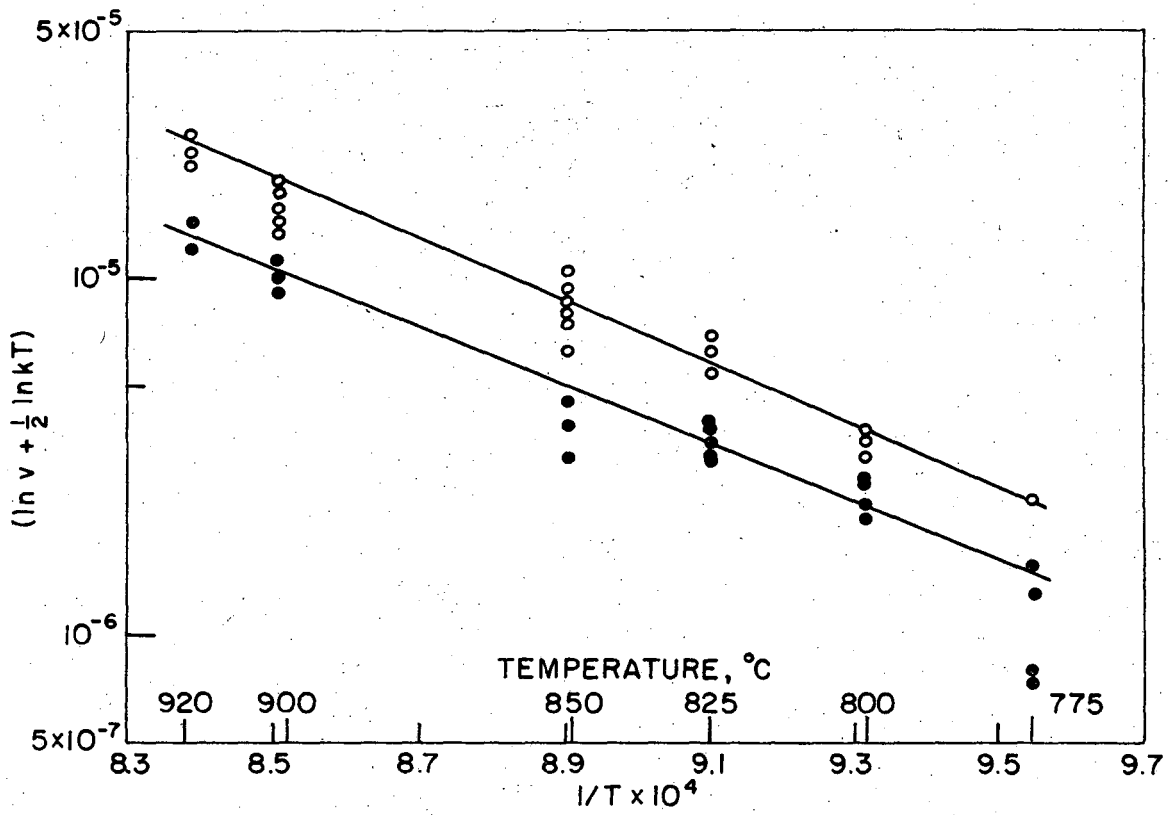

XBL 691-1

Fig. 27

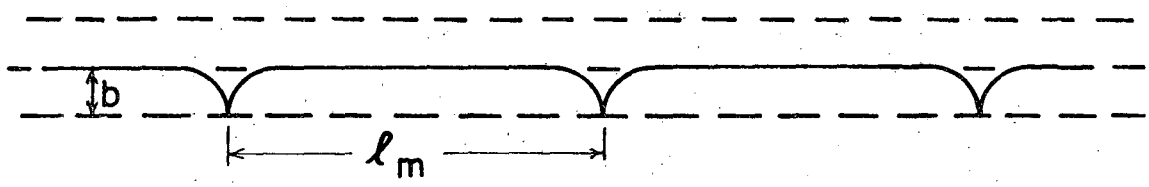

XBL 691-7

Fig. 28

LEGAL NOTICE

This report was prepared as an account of Government sponsored work. Neither the United States, nor the Commission, nor any person acting on behalf of the Commission:

A. Makes any warranty or representation, expressed or implied, with respect to the accuracy, completeness, or usefulness of the information contained in this report, or that the use of any information, apparatus, method, or process disclosed in this report may not infringe privately owned rights; or

B. Assumes any liabilities with respect to the use of, or for damages resulting from the use of any information, apparatus, method, or process disclosed in this report.

As used in the above, "person acting on behalf of the Commission" includes any employee or contractor of the Commission, or employee of such contractor, to the extent that such employee or contractor of the Commission, or employee of such contractor prepares, disseminates, or provides access to, any information pursuant to his employment or contract with the Commission, or his employment with such contractor.

TECHNICAL INFORMATION DIVISION
LAWRENCE RADIATION LABORATORY
UNIVERSITY OF CALIFORNIA
BERKELEY, CALIFORNIA 94720